iScience

CellPress
OPEN ACCESS

Article

Targeting SMYD3 to Sensitize Homologous Recombination-Proficient Tumors to PARP-Mediated Synthetic Lethality

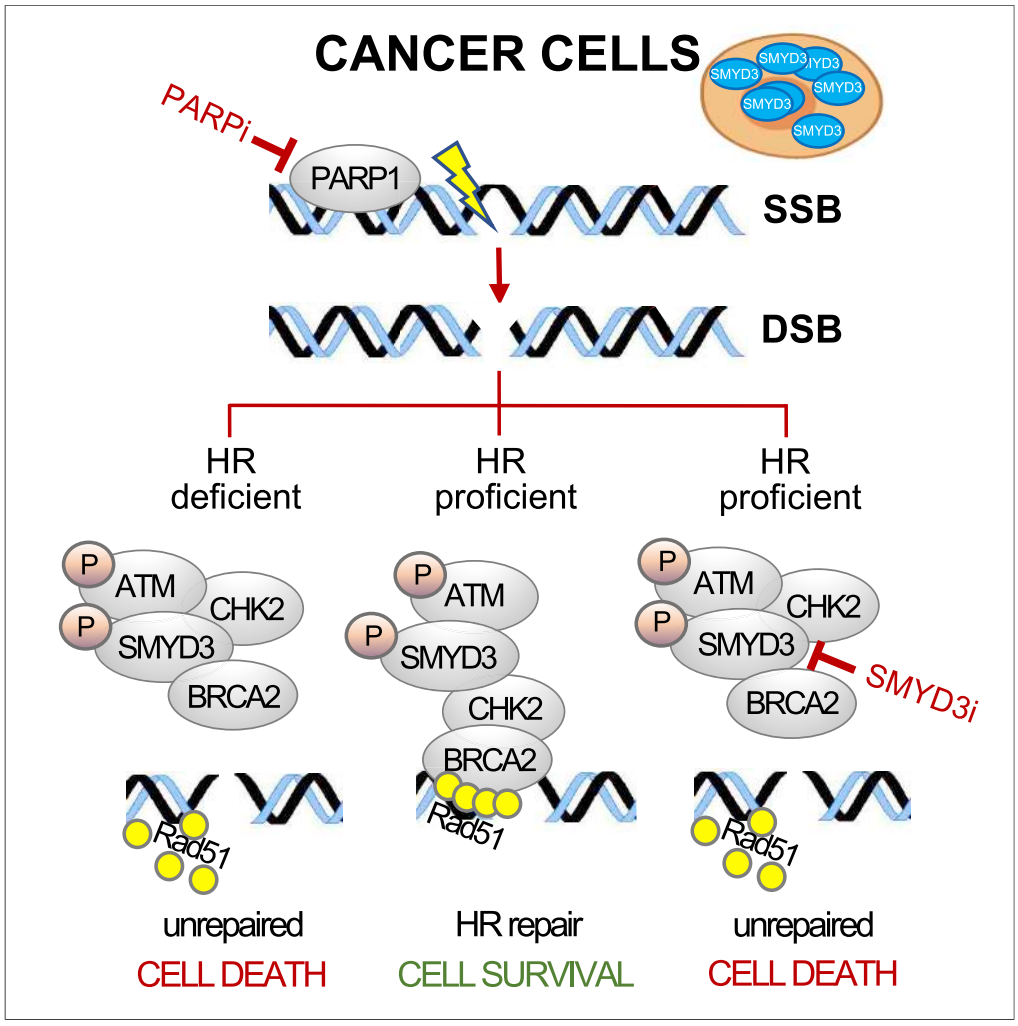

Paola Sanese, Candida Fasano, Giacomo Buscemi, ..., Giuseppina Caretti, Laura Ottini, Cristiano Simone

cristianosimone73@gmail.com

HIGHLIGHTS

SMYD3 phosphorylation by ATM favors the formation of HR complexes during DSB response

SMYD3 mediates DSB repair by promoting RAD51 recruitment at DNA damage sites

SMYD3 inhibition triggers a compensatory PARP-dependent DNA damage response

Co-targeting SMYD3/PARP leads to synthetic lethality in HR-proficient cancer cells

Sanese et al., iScience *23*, 101604
October 23, 2020
https://doi.org/10.1016/j.isci.2020.101604

iScience

CellPress
OPEN ACCESS

Article

Targeting SMYD3 to Sensitize Homologous Recombination-Proficient Tumors to PARP-Mediated Synthetic Lethality

Paola Sanese,[1,10] Candida Fasano,[1,10] Giacomo Buscemi,[2] Cinzia Bottino,[3] Silvia Corbetta,[3] Edoardo Fabini,[4,5] Valentina Silvestri,[6] Virginia Valentini,[6] Vittoria Disciglio,[1] Giovanna Forte,[1] Martina Lepore Signorile,[1] Katia De Marco,[1] Stefania Bertora,[1] Valentina Grossi,[1] Ummu Guven,[3] Natale Porta,[7] Valeria Di Maio,[7] Elisabetta Manoni,[5] Gianluigi Giannelli,[1] Manuela Bartolini,[4] Alberto Del Rio,[5,8] Giuseppina Caretti,[3] Laura Ottini,[6] and Cristiano Simone[1,9,11,*]

SUMMARY

***SMYD3* is frequently overexpressed in a wide variety of cancers. Indeed, its inactivation reduces tumor growth in preclinical *in vivo* animal models. However, extensive characterization *in vitro* failed to clarify *SMYD3* function in cancer cells, although confirming its importance in carcinogenesis. Taking advantage of a *SMYD3* mutant variant identified in a high-risk breast cancer family, here we show that SMYD3 phosphorylation by ATM enables the formation of a multiprotein complex including ATM, SMYD3, CHK2, and BRCA2, which is required for the final loading of RAD51 at DNA double-strand break sites and completion of homologous recombination (HR). Remarkably, SMYD3 pharmacological inhibition sensitizes HR-proficient cancer cells to PARP inhibitors, thereby extending the potential of the synthetic lethality approach in human tumors.**

INTRODUCTION

In recent years, the histone methyltransferase SET and MYND Domain containing 3 (SMYD3) gathered a lot of interest from researchers and pharmaceutical companies, and several SMYD3 chemical inhibitors were recently developed (Fabini et al., 2019a, 2019b; Bottino et al., 2020). Indeed, SMYD3 has been found overexpressed in colorectal cancer (CRC) as well as in other types of tumors, such as breast cancer (BC), ovarian cancer (OvCa), prostate cancer (PCa), pancreatic cancer (PC), gastric cancer, lung cancer, and hepatocellular carcinoma (Hamamoto et al., 2004, 2006; Tsuge et al., 2005; Mazur et al., 2014). SMYD3 has been initially identified as a member of the basal transcriptional machinery forming a complex with RNA polymerase II through the RNA helicase HELZ.3. This interaction, along with its ability to methylate histone tails at oncogene regulatory regions (Hamamoto et al., 2004, 2006; Zou et al., 2009; Sarris et al., 2016) and the increased susceptibility to some types of cancer conferred by the presence of tandem repeat polymorphisms in an E2F-binding element in its gene promoter (Tsuge et al., 2005), points to an oncogenic role for SMYD3. In normal cells, SMYD3 seems to be dispensable for development as well as for proliferation and survival. Indeed, SMYD3 homozygous conditional knockout (KO) mice, both male and female, did not show any significant abnormality after full phenotyping (http://www.informatics.jax.org/allele/key/571089; Mazur et al., 2014; Sarris et al., 2016). However, exogenous SMYD3 overexpression in normal cells is sufficient to accelerate cell growth and has a key role in the activation of genes acting downstream of pathways that are involved in tumor cell transformation and migration (Cock-Rada et al., 2012; Luo et al., 2014). It is worth noting that a number of sophisticated *in vivo* studies using SMYD3-KO mice models showed that this protein plays a key role in lung, pancreas, liver, and colon oncogenesis (Mazur et al., 2014; Sarris et al., 2016).

In a recently published work, we studied the expression and activity of SMYD3 in a CRC preclinical animal model and found that it is strongly upregulated throughout tumorigenesis both at the mRNA and protein levels. Our results also showed that RNAi-mediated SMYD3 ablation or its pharmacological blockade by a small-molecule inhibitor (BCI-121) induces a significant enrichment in the number of cancer cells in the S phase of the cell cycle (Peserico et al., 2015). Extended analysis revealed that SMYD3 is overexpressed

[1]Medical Genetics, National Institute of Gastroenterology "S. de Bellis" Research Hospital, Castellana Grotte, Bari 70013, Italy

[2]Institute of Molecular Genetics, IGM "Luigi Luca Cavalli-Sforza", National Research Council (CNR), Pavia 27100, Italy

[3]Department of Biosciences, University of Milan, Milan 20133, Italy

[4]Department of Pharmacy and Biotechnology, Alma Mater Studiorum University of Bologna, Bologna 40126, Italy

[5]BioChemoInformatics Unit, Institute of Organic Synthesis and Photoreactivity (ISOF), National Research Council (CNR), Bologna 40129, Italy

[6]Department of Molecular Medicine, University of Roma "La Sapienza", Roma 00185, Italy

[7]Department of Medical-Surgical Sciences and Biotechnology, Polo Pontino University of Roma "La Sapienza", Latina 04100, Italy

[8]Innovamol Consulting Srl, Modena 41123, Italy

[9]Department of Biomedical Sciences and Human Oncology (DIMO), Medical Genetics; University of Bari Aldo Moro, Bari 70124, Italy

[10]These authors contributed equally

[11]Lead Contact

*Correspondence: cristianosimone73@gmail.com

https://doi.org/10.1016/j.isci.2020.101604

in a wide variety of cancer cell lines, with cells expressing high levels of SMYD3 mRNA and protein (high SMYD3) being highly sensitive to its genetic depletion or pharmacological inhibition by BCI-121 (Peserico et al., 2015).

Several studies have been carried out to explore the mechanisms underlying SMYD3 oncogenic activity and suggest that, besides regulating gene expression-related processes, SMYD3 also interacts with and/or methylates non-histone proteins, through which it transactivates cancer-specific pathways. In the nucleus, SMYD3 interacts with heat shock protein 90 (HSP90), which modulates its binding to chromatin and activity (Hamamoto et al., 2004; Brown et al., 2015). SMYD3 also interacts with the PC4 coactivator, another component of the transcriptional machinery that promotes cell proliferation and invasion (Kim et al., 2015). Moreover, SMYD3 has been shown to interact with transcription factors involved in cancer, such as the estrogen receptor (ER), enhancing ER-mediated transcription (Kim et al., 2009). Additionally, it can methylate cytoplasmic proteins involved in signaling cascades that regulate cancer cell proliferation and survival, resulting in enhanced activation, as is the case for VEGFR1, AKT1, HER2, and the RAS/ERK signaling component MAP3K2 (Kunizaki et al., 2007; Yoshioka et al., 2016, 2017; Mazur et al., 2014). However, a recent work carried out by Thomenius and colleagues, who characterized *in vitro* hundreds of cancer cell lines by using several SMYD3 inhibitors (SMYD3is), SMYD3-specific siRNAs, and CRISPR/Cas9 KO cellular models, revealed that SMYD3's main contribution in the regulation of tumorigenesis is not based on simply sustaining autonomous proliferation of cancer cells but is still largely unknown (Thomenius et al., 2018). Intriguingly, it has been recently suggested that SMYD3 might participate in the homologous recombination (HR) pathway by modulating the expression of certain HR genes (Chen et al., 2017). HR is a multistep process that is tightly linked to human cancer risk. It is activated by the DNA damage sensor ATM and, through the sequential involvement of BRCA1, CHK2, and BRCA2, finally leads to RAD51 recombinase loading on chromatin at double-strand break (DSB) sites to repair these DNA lesions (Sun et al., 2020; Falck et al., 2005).

To get insight into SMYD3 functions in cancer cells, we performed a proteomic screening to find novel SMYD3 direct interactors that could help clarify its role in tumorigenesis. Here we report that SMYD3 is a direct interactor of the key members of the HR pathway, ATM, CHK2, and BRCA2, and is required for DSB repair. SMYD3 phosphorylation by ATM induces the formation of HR complexes and promotes the recruitment of RAD51 at DSB sites in response to endogenous damage or administration of DNA-damaging agents in CRC and BC cells. Finally, we show that targeting SMYD3 could help extend synthetic lethality approaches based on PARP inhibitors (PARPis) to HR-proficient tumors originating from different tissues.

RESULTS

SMYD3 Directly Interacts with ATM, CHK2, and BRCA2 *In Vitro* and *In Cellulo*

Based on the presence of a tetratricopeptide repeat module on SMYD3 C-terminal domain (Brown et al., 2015), we searched for new SMYD3-interacting proteins by screening tripeptides composed of rare amino acid residues, which are often found in specific interfaces for protein-protein interactions (Kanduc, 2010; Reiss and Schwikowski, 2004).

Therefore, we performed a peptide screening and identified a set of 19 short amino acid motifs (P-tripeptides) that were able to bind to SMYD3 *in vitro*, thus being eligible to be used as a minimum probe to screen the human proteome in the search for new SMYD3 interactors. Of note, all P-tripeptides were shown to interact with recombinant SMYD3 in a surface plasmon resonance (SPR) assay (Figure S1). No significant difference in binding responses between S-adenosyl methionine (SAM)-free and SAM-saturated binding events emerged, indicating there was no allosteric effect related to the presence of the methyl donor (SAM). Various proteomic studies suggest that rare amino acids often represent functional and/or protein-protein interaction consensus motifs (Kanduc, 2010; Kusalik et al., 2009) and that trimeric peptide modules act as biological effectors in protein-protein interactions (Wong et al., 2016; Kataya et al., 2015; Nam et al., 2014; Nishimura and Linder, 2013; Sudnitsyna et al., 2012; Kieken et al., 2009; Jeon et al., 2007). Thus, we performed an *in silico* analysis to investigate the specific distribution of these P-tripeptides in the human proteome, with the aim of identifying proteins with the highest number of P-tripeptide occurrences at functional sites as potential SMYD3 interactors. Surprisingly, the occurrence of P-tripeptides in all human proteins proved much lower than the theoretically expected probability value, suggesting that their distribution in the human proteome is not stochastic.

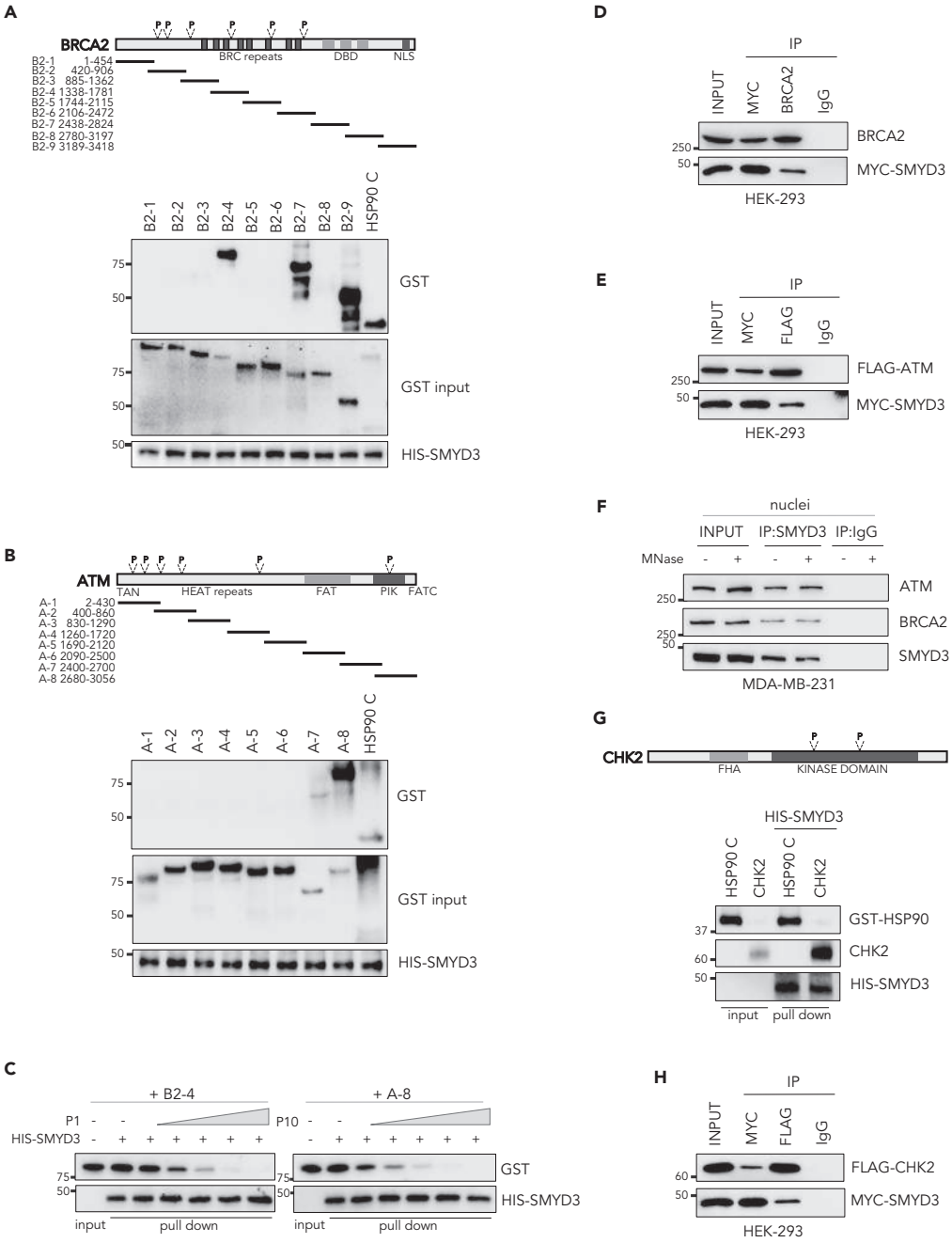

Figure 1. SMYD3 Directly Interacts with ATM, CHK2, and BRCA2 *In Vitro* and *In Cellulo*

(A) Upper panel: Diagram showing the nine overlapping GST-BRCA2 (B2-1 to B2-9) fusion proteins used in this study. Lower panel: HIS-SMYD3 bound to histidine beads was incubated with GST-BRCA2 fusion proteins and washed. Bound proteins were visualized by immunoblotting using anti-GST and anti-HIS antibodies.

(B) Upper panel: Diagram showing the eight overlapping GST-ATM (A-1 to A-8) fusion proteins used in this study. Lower panel: HIS-SMYD3 bound to histidine beads was incubated with GST-ATM fusion proteins and washed. Bound proteins were visualized by immunoblotting using anti-GST and anti-HIS antibodies.

(C) Competition assay: HIS-SMYD3 bound to histidine beads was incubated with GST-BRCA2 B2-4 and GST-ATM A-8 fusion proteins in the presence of escalating doses of the purified P1 and P10 tripeptides, respectively. Bound proteins were visualized by immunoblotting using anti-GST and anti-HIS antibodies.

(D) Co-immunoprecipitation assay in MYC-SMYD3- and BRCA2-overexpressing HEK-293 cells using anti-MYC and anti-BRCA2 antibodies.

Figure 1. *Continued*

(E) Co-immunoprecipitation assay in MYC-SMYD3- and FLAG-ATM-overexpressing HEK-293 cells using anti-MYC and anti-FLAG antibodies.

(F) Co-immunoprecipitation of endogenous SMYD3 using anti-SMYD3 antibodies in MDA-MB-231 nuclei treated with MNase to limit indirect interaction through polynucleosomes.

(G) Upper panel: Domain structure of CHK2 protein. Lower panel: HIS-SMYD3 bound to histidine beads was incubated with recombinant CHK2 protein and washed. Bound proteins were visualized by immunoblotting using anti-GST and anti-CHK2 antibodies.

(H) Co-immunoprecipitation assay in MYC-SMYD3- and FLAG-CHK2-overexpressing HEK-293 cells using anti-MYC and anti-FLAG antibodies.

(A, B, C, and G) A 10% input of the purified fusion proteins was used as a loading control. (A, B, and G) GST-HSP90 C-terminal (616–736) was used as a positive control. (D, E, F, and H) Anti-IgGs were used as negative controls.

P, P-tripeptide. Results are representative of at least three independent experiments. See also Figures S1 and S2.

Indeed, our screening showed that among 169,671 reviewed human proteins (analysis performed in December 2018; www.uniprot.org, UniProt Consortium, 2014), only 8,650 (5.1%) contain at least one P-tripeptide. Intriguingly, we found $\geq$4 P-tripeptide occurrences in only 214 (0.12%) proteins, which represented our starting subset to identify new potential SMYD3 interactors. One of these 214 proteins was VEGFR1, a known SMYD3 interactor and substrate (Kunizaki et al., 2007). After clustering the selected proteins for their biological role, we observed an enrichment in the cluster involved in DNA repair and S-phase checkpoint (Figure S2). Then, we searched for members of the HR pathway (Reactome database, http://reactome.org.), as it has been proposed that SMYD3 might regulate the expression of certain HR genes (Chen et al., 2017). The best candidates identified by our *in silico* analysis were BRCA2 and ATM (with 6 P-tripeptide matches each). BRCA2 is a critical protein in the HR process for DSB repair (Krejci et al., 2012); it has been found mutated in various cancers (BC, OvCa, PC, CRC), and its germline mutations specifically predispose to breast and ovarian cancers (Petrucelli et al., 2010). First, we analyzed *in vitro* the interaction between a full-length HIS-tagged SMYD3 recombinant protein and a series of nine GST fusion proteins, designated B2-1 to B2-9 (Lee et al., 2004), which span the entire BRCA2 coding region (Figure 1A). Interestingly, HIS pull-down assay results showed that BRCA2 B2-4, B2-7, and B2-9 fragments interact with SMYD3 (Figure 1A). These fragments encompass BRC repeats and the C-terminal domain, which mediate RAD51 binding and regulation on resected DNA substrates (Carreira et al., 2009; Chatterjee et al., 2016). These results validated the predictions of our proteomic screening by showing that BRCA2-SMYD3 interaction occurs directly and specifically involves at least one region (B2-4) encompassing a P-tripeptide motif.

ATM is the initiator kinase mediating DNA DSB response through activation of the HR cascade (You et al., 2007; Lee and Paull, 2007). We thus performed an ATM-SMYD3 *in vitro* pull-down assay by using HIS-tagged SMYD3 and eight GST-ATM fusion proteins, designated A-1 to A-8 (Takai et al., 2007), and found that A-7 and A-8 fragments interact with SMYD3 (Figure 1B). These two consecutive fragments encompass ATM phosphatidylinositol kinase (PIK) domain, which mediates its kinase activity (Bakkenist and Kastan, 2003) and contains one P-tripeptide.

To validate the involvement of the identified tripeptide motifs in SMYD3 interaction, we performed an *in vitro* competition assay for SMYD3 binding between the BRCA2/ATM fragments containing the relevant tripeptide sequences and the specific purified P-tripeptides. Specifically, we tested BRCA2 GST-B2-4 fragment (encompassing P1, NFF) with escalating doses of the purified P1 tripeptide and ATM GST-A-8 fragment (encompassing P10, NDF) with escalating doses of the purified P10 tripeptide. In both cases, the purified P-tripeptides interfered with the binding between HIS-SMYD3 and the indicated BRCA2/ATM fragments in a dose-dependent manner (Figure 1C).

Next, we assessed whether a direct interaction between SMYD3 and ATM or BRCA2 also occurs *in cellulo*. Co-immunoprecipitation (coIP) assays in HEK-293 cells transiently transfected with Myc-tagged SMYD3 and BRCA2 or FLAG-ATM confirmed the results obtained *in vitro* (Figures 1D and 1E). To validate these findings, we also performed coIP assays of the endogenous proteins in breast cancer MDA-MB-231 cells, which express high levels of SMYD3 (Figure S3A) and are wild-type for both ATM and BRCA2 (Figure S5F), in the presence or absence of MNase to rule out indirect interaction via chromatin. Our results showed similar signals in both experimental conditions, confirming that SMYD3 directly interacts with BRCA2 and ATM (Figure 1F).

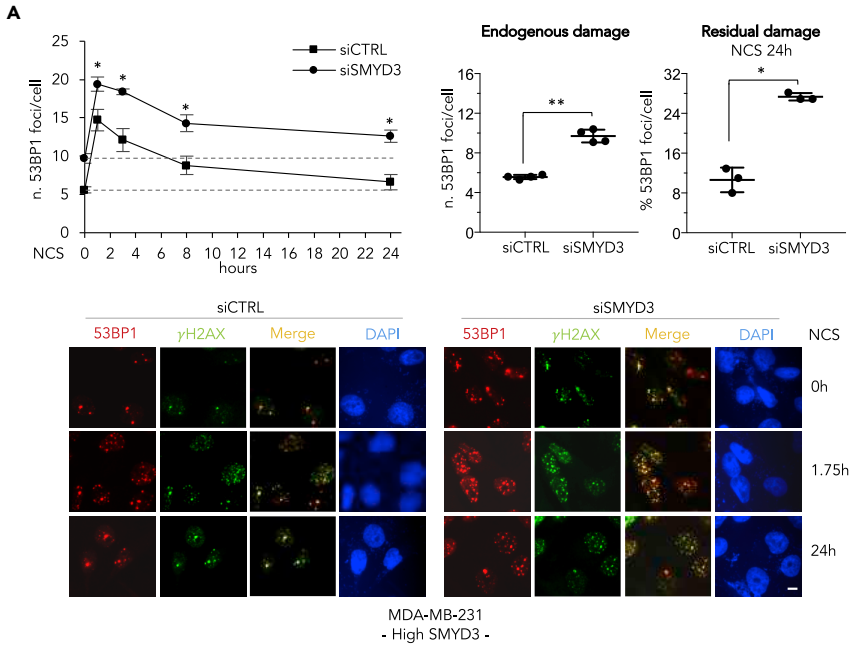
A
n. 53BP1 foci/cell
siCTRL
siSMYD3
NCS
hours
Endogenous damage
Residual damage
NCS 24h
% 53BP1 foci/cell
siCTRL
siSMYD3
53BP1
γH2AX
Merge
DAPI
NCS
0h
1.75h
24h
MDA-MB-231
- High SMYD3 -

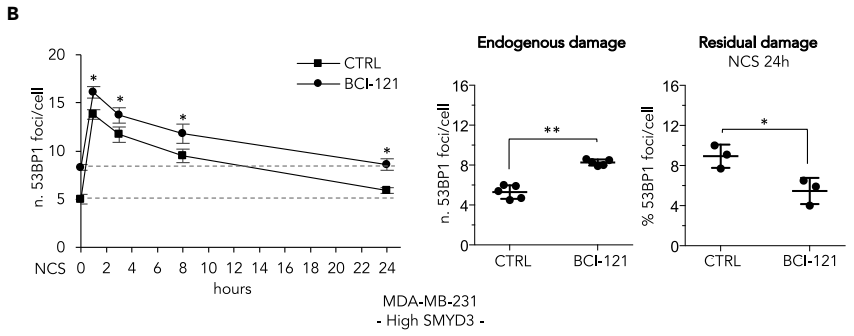
B
n. 53BP1 foci/cell
CTRL
BCI-121
NCS
hours
Endogenous damage
Residual damage
NCS 24h
% 53BP1 foci/cell
MDA-MB-231
- High SMYD3 -

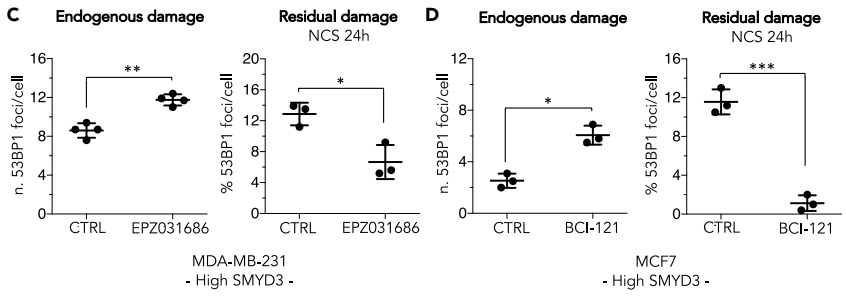
C
Endogenous damage
Residual damage
NCS 24h
n. 53BP1 foci/cell
% 53BP1 foci/cell
CTRL
EPZ031686
MDA-MB-231
- High SMYD3 -
D
Endogenous damage
Residual damage
NCS 24h
n. 53BP1 foci/cell
% 53BP1 foci/cell
CTRL
BCI-121
MCF7
- High SMYD3 -

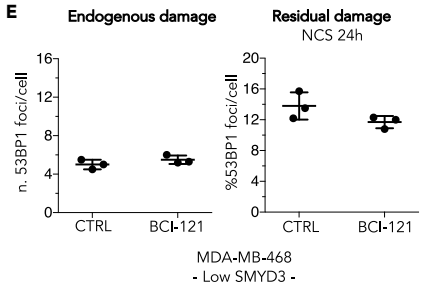
E
Endogenous damage
Residual damage
NCS 24h
n. 53BP1 foci/cell
%53BP1 foci/cell
CTRL
BCI-121
MDA-MB-468
- Low SMYD3 -

Figure 2. SMYD3 Mediates DSB Repair in BC Cells

(A) High-SMYD3 MDA-MB-231 cells were transfected with control (siCTRL) or SMYD3-specific (siSMYD3) siRNAs, exposed to 0.8 nM neocarzinostatin (NCS) after 48 h, and fixed at the indicated time points. Upper panel: Number of 53BP1 foci/cell based on immunostaining for 53BP1. At least 100 cells were analyzed for each time point. Means and standard deviations obtained from at least three independent experiments are shown in the graph on the left. The graph in the middle shows the number of 53BP1 foci/cell before NCS addition (endogenous damage). The graph on the right shows the percentage of 53BP1 foci/cell induced by NCS and detectable 24 h after drug exposure (residual damage NCS 24h). Lower panel: double immunostaining for 53BP1 (red) and γH2AX (green). Nuclei were stained with DAPI (blue). Representative images are shown. The scale bar represents 5 μm.

(B) MDA-MB-231 cells were treated with 10 μM BCI-121 2.5 h before NCS addition. Immunostaining for 53BP1 and foci counting were performed and are graphically shown as in (A).

(C) Same as in (B) but cells were treated with 1 μM EPZ031686.

(D and E) Same as in (B), but experiments were performed on high-SMYD3 MCF7 cells (D) and low-SMYD3 MDA-MB-468 cells (E).

Data are presented as mean (SD), and significance was calculated using Student's t-test; *$p < 0.05$, **$p < 0.01$, and ***$p < 0.001$. Results are representative of at least three independent experiments.

See also Figure S3.

These findings prompted us to further explore our screening list in the search for other key players of the HR pathway. Interestingly, we found that CHK2, a kinase that acts downstream of ATM and plays an effector role in the HR pathway by activating BRCA2 (Shiloh, 2003), also contains 2 P-tripeptides. Our data indicate that CHK2 can also interact with SMYD3 both *in vitro* and *in cellulo* (Figures 1G and 1H).

SMYD3 Mediates DSB Repair in BC Cells

To assess SMYD3 direct involvement in the HR repair process, we analyzed the formation and clearance of nuclear foci of the damage sensor p53-binding protein 1 (53BP1), a DSB marker (Panier and Boulton, 2014). Since we found that SMYD3 is overexpressed in a large panel of BC cell lines (Figure S3A), including triple-negative breast cancer (TNBC) cells (a BC phenotype for which no standard therapy is currently recommended), we genetically silenced SMYD3 in the high-SMYD3 TNBC cell line MDA-MB-231 and evaluated 53BP1 foci in non-stressed asynchronous cells. Double-immunostaining experiments for foci containing 53BP1 and γH2AX, which is another DSB response component that co-localizes with 53BP1, revealed the presence of a higher number of 53BP1/γH2AX-positive foci in cells treated with SMYD3-specific siRNAs, indicating the presence of increased unrepaired endogenous DSB lesions in SMYD3-depleted cells (Figures 2A and S3B). An increase in 53BP1 foci was also observed when cells were treated with the SMYD3 inhibitors BCI-121 or EPZ031686 for 2.5 h (Figures 2B and 2C). Next, we determined the ability of SMYD3-interfered cells to repair neocarzinostatin (NCS)-induced DSBs (Dedon and Goldberg, 1992). Twenty-four hours after NCS exposure, cells that were genetically depleted for SMYD3 were incapable of completely repairing DNA compared with non-silenced cells (Figure 2A). This evidence indicates that SMYD3 genetic ablation prevents correct repair and resolution of DSBs at this time point (Figure 2A). In contrast, SMYD3i treatment did not affect the resolution of NCS-induced DNA lesions in MDA-MB-231 cells at the 24-h time point (Figures 2B and 2C). Similar results were obtained when 53BP1 foci were analyzed both in unstressed conditions and following NCS exposure in BCI-121-treated MCF7 cells, a different high-SMYD3 BC cell line (Figure 2D). Importantly, BCI-121 treatment did not affect the abundance of endogenous or NCS-induced 53BP1 foci in the MDA-MB-468 cell line, in which SMYD3 expression is barely detectable (low SMYD3) (Figure 2E). These findings confirmed that *SMYD3* has a critical role in DSB repair and its protein expression is required for DNA restoration. However, although its function appears to be critical for endogenous damage, data related to residual damage after NCS exposure suggest that alternative DNA repair mechanisms might be involved when SMYD3 is pharmacologically impaired.

Of note, the results obtained upon 2.5 h pre-treatment with a SMYD3i (Figures 2B–2D) indicate that, at least in cancer cells, the main role of SMYD3 in DSB repair is not the epigenetic regulation of certain HR genes as previously suggested (Chen et al., 2017) but involves an important transcription-independent activity that positively mediates DSB repair in cancer cells expressing high levels of SMYD3.

SMYD3 Analysis in the Pan-Cancer Dataset and Identification of a Genetic Variant in a High-Risk BC Family

The involvement of SMYD3 in HR, together with its interaction with ATM, CHK2, and BRCA2, which are all encoded by genes that are highly mutated in sporadic cancers and are implicated in genetic predisposition

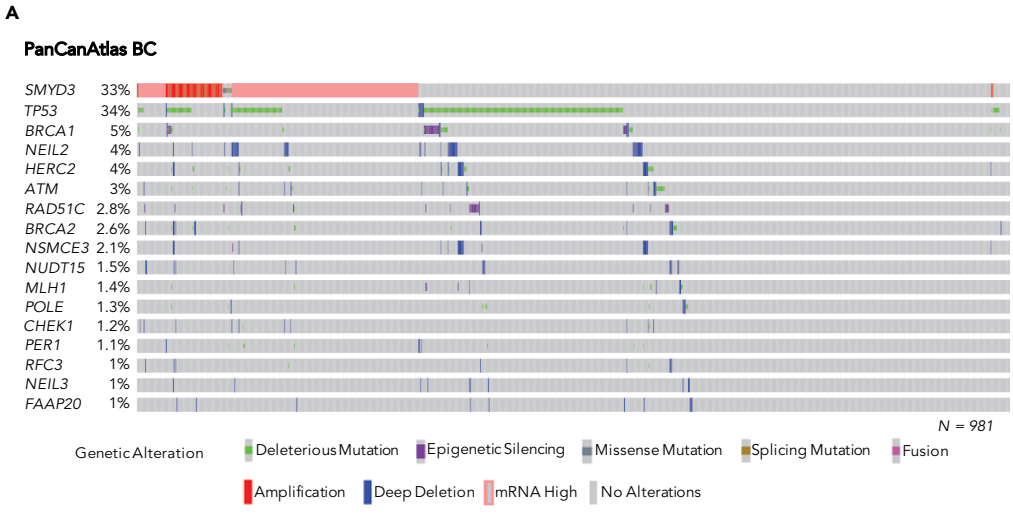

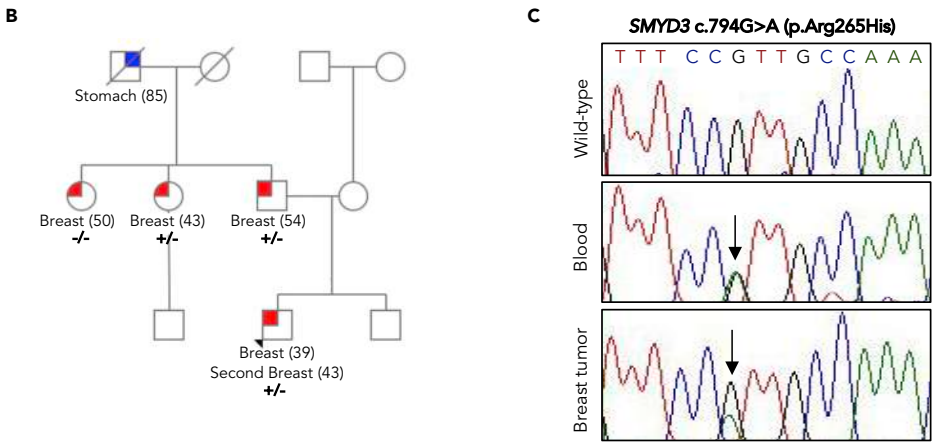

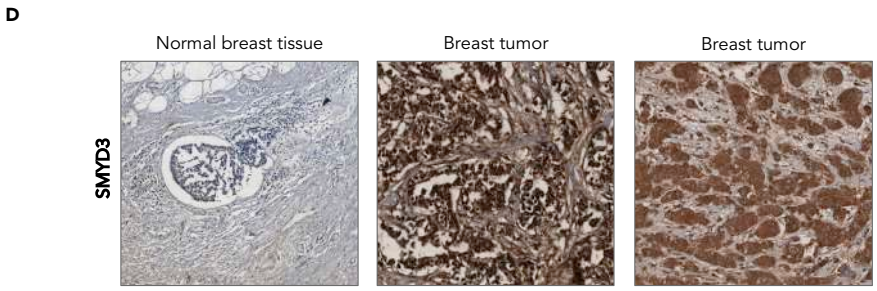

Figure 3. SMYD3 Analysis in the PanCanAtlas BC Dataset and Identification of a Genetic Variant in a High-Risk BC Family

(A) Oncoprint of *SMYD3* and HRD-associated genes in PanCanAtlas BC tumors. Overall profiling of 981 BC tumors (columns) carrying alterations involving the *SMYD3* gene (mRNA overexpression, copy number alterations, and mutations) and deleterious mutations, deletions, and epigenetic silencing events for each HRD-associated gene (rows with gene names listed on the left) in more than 1% of cases. Gray boxes indicate the absence of alterations, and color/shape combinations corresponding to the various alteration types are indicated below the oncoprint. The overall frequency of each gene alteration in the oncoprint plot is indicated on the left.

(B) Pedigree of the BC family selected for whole-exome sequencing. The proband is indicated by an arrowhead. For each individual diagnosed with cancer, the age at diagnosis is reported. Tested family members are marked as +/− to indicate *SMYD3* (C)794G>A (p.Arg265His) heterozygous mutation carriers or as −/− to indicate wild-type *SMYD3* individuals.

(C) Partial electropherogram of *SMYD3* exon 8 confirming the presence of the *SMYD3* c.794G>A mutation (indicated by a black arrow) in both the germline and the tumor DNA of the proband.

Figure 3. *Continued*
(D) SMYD3 expression by immunohistochemistry in normal male breast tissue (left) and male breast tumors: cytoplasmic only localization (center) and nuclear and cytoplasmic localization (right). All the analyzed BC sections showed strong (3+) SMYD3 expression compared with normal breast tissue, regardless of *SMYD3* mutational status. Magnification: 20×. Results are representative of at least three independent experiments. See also Figure S4 and Table S1.

to BC (Jerzak, et al., 2018; Apostolou and Papasotiriou, 2017; Tazzite, et al., 2020), prompted us to analyze *SMYD3* genomic alterations and mRNA expression using publicly available human breast invasive carcinoma data from The Cancer Genome Atlas (TCGA) Pan-Cancer dataset. We included in this study a total of 981 primary tumors previously and systematically analyzed by integrating data on somatic truncating mutations, deep copy-number deletions, and epigenetic silencing events involving a curated list of 276 genes encompassing all major DNA repair pathways (Knijnenburg et al., 2018). We used the cBioPortal website (http://www.cbioportal.org) to assess somatic alterations involving the *SMYD3* gene in 981 selected BC tumors. Tumors were stratified based on *SMYD3* RNA-seq *Z* score, and the third quartile was identified as high SMYD3 (q3: *SMYD3 Z* score $\geq$ 1.06). This analysis revealed that the overall frequency of somatic alterations involving the *SMYD3* gene was of about 33% in all BC tumors. Specifically, a low proportion of BC tumors (11/981; 1.12%) harbored missense (6/981), fusion (1/981), or deleterious (4/981) mutations involving the *SMYD3* gene. Among the six *SMYD3* missense mutations identified in the BC dataset, two (c.203C>T, p.Ala68Val; c.620G>T, p.Ser207Ile) were identified in diploid tumors with low/normal *SMYD3* mRNA levels and were predicted to be probably deleterious by *in silico* analysis. Furthermore, in agreement with the observation that SMYD3 is overexpressed in several cancer types (Zhu and Huang, 2020; Bottino et al., 2020), increased *SMYD3* mRNA levels were observed in 25% of BC tumors (245/981); of these, 32 also harbored copy number amplifications. The presence of copy number amplifications involving the *SMYD3* gene was observed in 6.7% of all BC tumors (66/981). These data highlighted the role of SMYD3 overexpression in the pathogenesis of sporadic BC (Figures 3A and S4).

Next, we investigated whether *SMYD3* could also be involved in genetic susceptibility to inherited BC. To this aim, we focused on a high-risk BC family who tested negative for *BRCA1/2* germline mutations and comprised four patients with BC, two males and two females (Figure 3B), selected from the ongoing Italian Multicenter Study on Male Breast Cancer (MBC) (Rizzolo et al., 2019). Whole-exome sequencing was performed on the germline DNA of the two MBC patients. A rare *SMYD3* missense variant (c.794G>A; p.Arg265His; rs61762672), which was predicted to be potentially pathogenic by *in silico* analysis, was found in both MBC patients (Figure 3C). Sequencing analysis of tumor DNA isolated from all four patients with BC showed that the two males and one of the females harbored this variant (Figure 3C). Further analysis of transcriptome data of one of the two BC males showed that the *SMYD3* p.Arg265His variant and the wild-type allele were expressed in the tumor with similar percentages (the variant allele and the wild-type allele represented 43% and 57% of the total reads, respectively). SMYD3 protein immunohistochemical expression was evaluated in BC samples from all four affected family members. Strong (3+) SMYD3 expression was detected in tumor cells; by contrast, tumor-surrounding normal breast tissue exhibited weak/absent immunostaining (Figure 3D). Tumor samples displayed $\geq$70% SMYD3-positive cells: 95% in BC samples derived from family members with the germline *SMYD3* p.Arg265His variant and 70% in the sample from the *SMYD3* wild-type family member. SMYD3 immunostaining was detected both in the nucleus and in the cytoplasm, showing variable cellular localization across BC samples. Specifically, SMYD3 showed either cytoplasmic or cytoplasmic/nuclear localization in BC samples derived from family members with the germline *SMYD3* p.Arg265His variant, whereas it displayed cytoplasmic only localization in the BC sample from the *SMYD3* wild-type family member (Table S1 and Figure 3D). Overall, both RNA and protein expression data in BC samples suggest that the *SMYD3* p.Arg265His variant could be a rare missense mutation acting with a dominant-negative effect on the wild-type protein.

SMYD3 Promotes the Formation of HR Complexes during DSB Response and Is a Substrate of ATM

Identification of the *SMYD3* p.Arg265His variant prompted us to gain further molecular details on SMYD3 function in the HR pathway. To this end, we characterized this variant in our models. We first examined the role of wild-type SMYD3 (SMYD3-WT) in the formation of HR complexes by transfecting HEK-293 cells (Low SMYD3, Figure S3A) with a vector expressing FLAG-tagged SMYD3-WT. CoIP with anti-FLAG antibodies revealed that SMYD3-WT can bind to the HR complex members ATM, CHK2, BRCA2, and RAD51 following DNA damage induced by doxorubicin exposure, and ATM pharmacological inhibition affects this

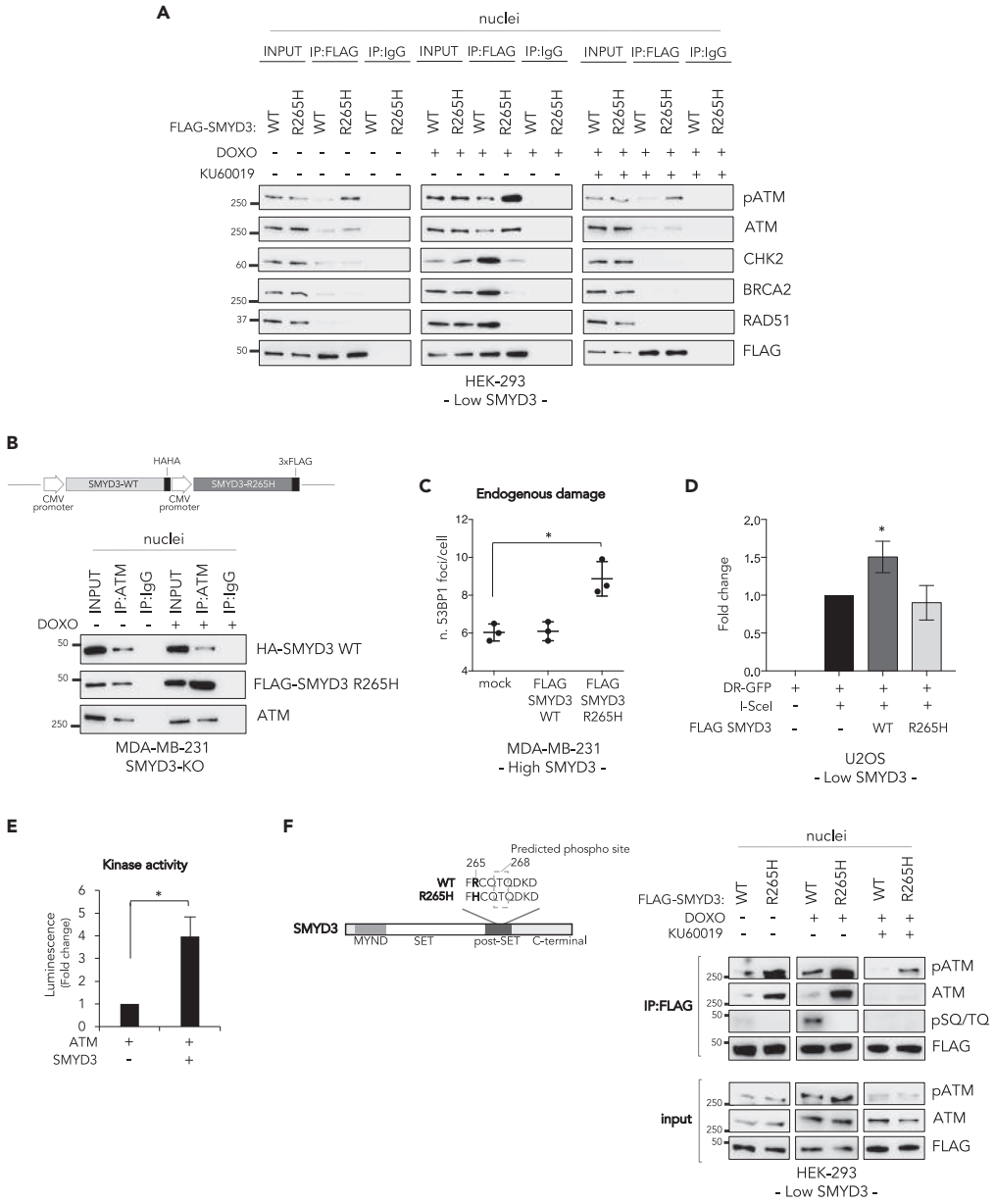

Figure 4. SMYD3 Promotes the Formation of HR Complexes during DSB Response and Is a Substrate of ATM

(A) Co-immunoprecipitation assay with anti-FLAG antibodies in nuclear fractions from HEK-293 cells transfected with FLAG-SMYD3-WT or FLAG-SMYD3-R265H after treatment with doxorubicin (1 μM) and/or the ATM inhibitor KU60019 (1 μM) for 6 h.

(B) Upper panel: Schematic representation of the plasmid coding for both HA-SMYD3-WT and FLAG-SMYD3-R265H used in the subsequent assay. Lower panel: Co-immunoprecipitation assay with anti-ATM antibodies in nuclear fractions from SMYD3-KO MDA-MB-231 transfected cells after doxorubicin exposure (1 μM, 6 h). (A, B) Anti-IgGs were used as negative controls.

(C) After 48 h of transfection with the indicated constructs, high-SMYD3 MDA-MB-231 cells were fixed and immunostained with an anti-53BP1 antibody in combination with an anti-FLAG antibody. Cells positive for FLAG-SMYD3 nuclear staining were considered for 53BP1 counting. At least 50 cells were analyzed in each of three independent experiments. Data shown in the graph (endogenous damage) are presented as mean (SD).

(D) U2OS DR-GFP cells were transfected with the I-SceI and the indicated SMYD3 expression plasmids. After 24 h of transfection the percentage of GFP+ cells was determined for each condition by FACS and subsequently normalized to the control cells. Data are presented as the mean (SD) (n = 3). Significance was determined by one-way ANOVA followed by a Dunnett test. *p < 0.05.

Figure 4. *Continued*

(E) *In vitro* kinase assay showing SMYD3 phosphorylation by ATM, as measured by the luminescence signal resulting from ADP generation.

(F) Left panel: Schematic representation of the human SMYD3 protein highlighting the domains and residues located around the identified variant. The dotted square indicates the ATM phosphorylation site (Thr 268) based on *in silico* predictions by three different tools (http://phospho.elm.eu.org/; http://www.dabi.temple.edu/disphos/; http://www.cbs.dtu.dk/services/NetPhos/). Right panel: Co-immunoprecipitation assay with anti-FLAG antibodies in nuclear fractions from HEK-293 cells transfected with FLAG-SMYD3-WT or FLAG-SMYD3-R265H after treatment with doxorubicin (1 μM) and/or the ATM inhibitor KU60019 (1 μM) for 6 h.

Significance was calculated using Student's t-test; *$p < 0.05$. DOXO, doxorubicin. Results are representative of at least three independent experiments.

See also Figure S3.

interaction (Figure 4A). These results showed that SMYD3 is part of the HR complex and may mediate its assembly and/or activity. The novel interaction with RAD51 emerging from this experiment, which is consistent with the observation that SMYD3 interacts with BRCA2 regions involved in RAD51 binding (Figure 1A), suggests that SMYD3 may recruit RAD51 on resected DNA ends as a final readout of DNA repair signals. Transfection of HEK-293 cells with a vector expressing the FLAG-tagged *SMYD3* p.Arg265His variant (SMYD3-265H) showed that this variant binds to ATM, especially in its phosphorylated form, with a higher affinity than SMYD3-WT but loses the ability to bind other members of the complex (Figure 4A). These data suggest that the *SMYD3* p.Arg265His variant might have a dominant-negative activity on ATM and may impair SMYD3 ability to modulate DNA repair. To test this hypothesis, we first generated a SMYD3-KO MDA-MB-231 cell line (MDA-MB-231 SMYD3-KO) using the CRISPR-Cas9 system for genome editing, along with a vector expressing both HA-tagged SMYD3-WT and FLAG-tagged SMYD3-R265H. Then, we transfected SMYD3-KO MDA-MB-231 cells with this vector and performed coIP assays with anti-ATM antibodies. After induction of DNA damage with doxorubicin, we found that ATM binds SMYD3-R265H with higher affinity than SMYD3-WT (Figure 4B). Moreover, analysis of 53BP1 foci in the high-SMYD3 cell line MDA-MB-231 transfected with FLAG-SMYD3-WT or FLAG-SMYD3-R265H revealed that increased endogenous DSBs are found in cells overexpressing the mutant form (Figure 4C). These latter results were further confirmed by a DR-GFP reporter assay, in which the I-SceI endonuclease is expressed in low-SMYD3 U2OS cells (Figure S3A) that are integrated with a direct repeat DR-GFP. I-SceI generates a DSB that restores GFP expression when repaired by HR (Gunn and Stark, 2012; Pierce et al., 1999). This assay showed that SMYD3-WT overexpression in the presence of I-SceI promoted HR repair efficiency and that this increase was not detectable when the SMYD3-R265H mutant was co-transfected (Figure 4D).

These data indicate that the *SMYD3* p.Arg265His variant exerts a dominant-negative activity resulting in the accumulation of unrepaired DNA, an effect possibly mediated by enhanced ATM binding. These findings suggest that SMYD3 could be a substrate of ATM. To verify this hypothesis, we performed an *in vitro* kinase assay using the purified proteins. Our results showed that active ATM can efficiently phosphorylate SMYD3 (Figure 4E). Intriguingly, an *in silico* analysis suggested that the best candidate site for ATM phosphorylation is T268, a residue that is very close to the mutation site (R265H) we identified in the high-risk BC family (Figure 4F). To ascertain whether ATM can also phosphorylate SMYD3-R265H *in cellulo*, we transfected HEK-293 cells with a vector expressing FLAG-tagged SMYD3-WT or FLAG-tagged SMYD3-R265H and performed coIP assays with anti-FLAG antibodies. Phosphorylation of SMYD3-WT following doxorubicin exposure was observed with phospho-specific SQ/TQ antibodies, which recognize proteins phosphorylated on these motifs. This site was specifically targeted by ATM, as confirmed by the loss of phosphorylation observed after ATM inhibition. Remarkably, no phosphorylation was detected in cells overexpressing the mutant form SMYD3-R265H (Figure 4F).

SMYD3 Localizes at DSBs and Its R265H Mutation Prevents RAD51 Recruitment

Because of SMYD3 ability to associate to chromatin (Peserico et al., 2015; Sarris et al., 2016; Fenizia, et al., 2019; Proserpio et al., 2013), we wondered whether it is recruited at DSBs. First, we performed chromatin immunoprecipitation (ChIP) assays in low-SMYD3 DR-GFP U2OS cells (Figure S3A) transfected with FLAG-SMYD3-WT or empty vectors and we found that FLAG-SMYD3-WT associates to chromatin in close proximity to the DSB (Figure 5A). Of note, ATM pharmacological inhibition prevented the recruitment of SMYD3 at the DSB site (Figure 5A), thus confirming the role of ATM-dependent SMYD3 phosphoactivation in the assembly of the HR multiprotein complex (Figures 4A and 4E).

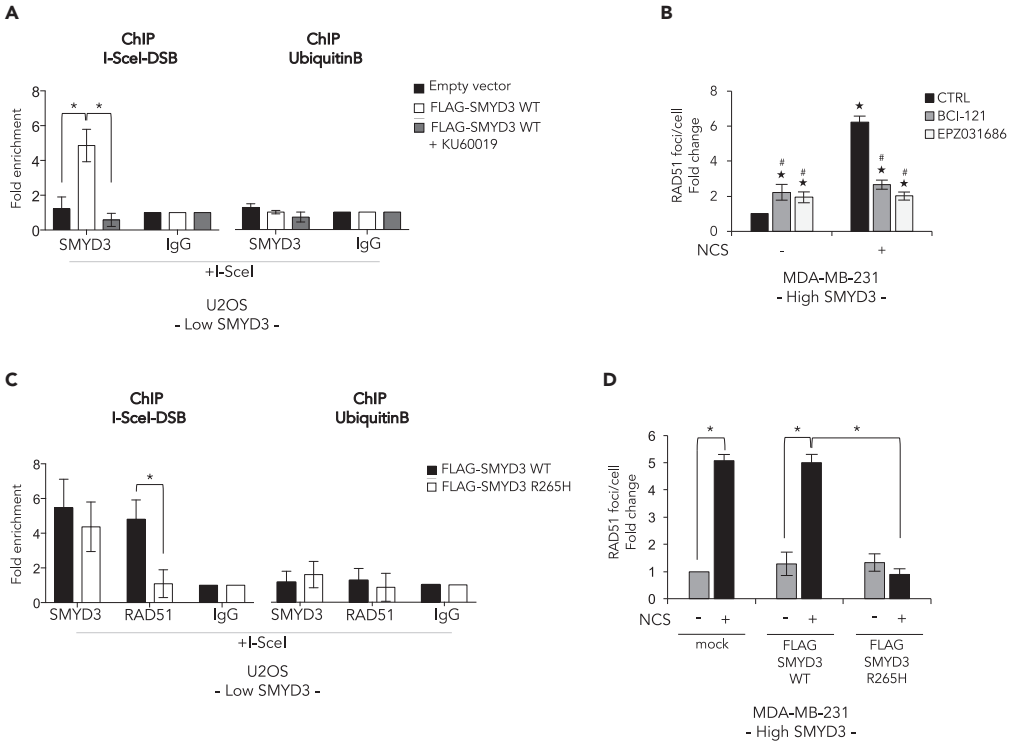

Figure 5. SMYD3 Localizes at DSBs and Its R265H Mutation Prevents RAD51 Recruitment

(A) SMYD3 association to DSB regions was assayed by chromatin immunoprecipitation (ChIP) qPCR in DR-GFP U2OS cells transiently co-transfected with a plasmid carrying the I-SceI coding sequence and either an empty vector or the FLAG-SMYD3-WT plasmid and treated or not with KU60019 (1 μM). ChIP assays were performed using antibodies against SMYD3, and the region +1300 bp from the cut site was analyzed by qPCR.

(B) MDA-MB-231 cells were pre-treated for 4 h with BCI-121 (30 μM) or EPZ031686 (1 μM) and then subjected to DNA damage with NCS (1 nM) for 6 h. The graph reflects the quantification of RAD51 foci analyzed by immunofluorescence. ★p ≤ 0.05, all treatments compared with control (-NCS); #p ≤ 0.05, SMYD3i treatment compared with its respective control (±NCS).

(C) DR-GFP U2OS cells were transiently co-transfected with a plasmid coding for I-SceI and either FLAG-SMYD3-WT or the FLAG-SMYD3-R265H variant. ChIP assays were performed using antibodies against SMYD3 and RAD51, and the region +1300 bp from the cut site was analyzed by qPCR.

(D) MDA-MB-231 cells were transfected with FLAG-SMYD3-WT or FLAG-SMYD3-R265H and then treated with NCS (1 μM) for 6 h. The graph reflects the quantification of RAD51 foci analyzed by immunofluorescence.

(A and C) The ubiquitin B promoter was used as a negative control. Data are expressed as fold enrichment compared with IgGs and represent means (SD).

Statistical analysis was performed using Student's t-test: *p ≤ 0.05 was considered statistically significant. Results are representative of at least three independent experiments. See also Figures S3 and S5.

Based on these findings, we tested the hypothesis that SMYD3 might be involved in RAD51 loading on DSBs by analyzing RAD51 foci in MDA-MB-231 cells treated or not with BCI-121 or EPZ031686. We found that SMYD3 inhibition impairs the formation of RAD51 foci on DSBs after NCS exposure (Figures 5B and S5A).

Since the SMYD3-R265H mutant strongly binds to (phospho-)ATM but failed to interact with CHK2, BRCA2, and RAD51 in doxorubicin-treated cancer cells (Figure 4A), we assessed whether it could be recruited at DSB sites. To this end, we performed a ChIP assay in low-SMYD3 DR-GFP U2OS cells overexpressing FLAG-SMYD3-WT or FLAG-SMYD3-R265H and observed that both proteins occupy the DNA break region. However, in SMYD3-WT-overexpressing cells RAD51 co-occupied the break site, whereas overexpression of FLAG-SMYD3-R265H dramatically impaired RAD51 recruitment in proximity to the damage (Figure 5C). Consistent with the dominant-negative effect of FLAG-SMYD3-R265H overexpression observed in MDA-MB-231 cells (Figure 4C), our results showed that the mutant variant impairs RAD51 loading at DSBs after damage (Figures 5D and S5B).

Overall, these data suggest that SMYD3 associates with DSBs and the R265H variant does not affect SMYD3 localization at these sites but prevents proper HR complex formation and RAD51 recruitment at DSBs.

SMYD3 Inhibition Triggers a Compensatory PARP-Dependent DNA Damage Response

We observed a difference between the effect of SMYD3 genetic ablation or pharmacological inhibition on the residual damage of BC cells exposed to a DNA damaging agent, as reported in Figure 2. These findings prompted us to analyze in depth the possibility that other DNA repair signals may be activated to restore efficient DSB religation in the presence of a SMYD3i. PARP1 is an important player in DNA damage response: it acts upstream of various pathways and is implicated both in single-strand break repair mechanisms and in the regulation of DSB repair (Pascal, 2018). Thus, in order to investigate the potential compensatory effect of DNA repair mechanisms, other than HR, acting in BC cells treated with NCS and a SMYD3i, we inhibited PARP in these cells by using olaparib, an FDA-approved PARPi for BRCA1/2-mutated ovarian and pancreatic tumors (Buchtel et al., 2018). We first analyzed 53BP1 foci in MDA-MB-231 cells pre-treated with a SMYD3i alone, olaparib alone, or a combination of both, followed by 24 h NCS exposure in order to induce DSBs (Figure 6A, right panel, and S5C). Of note, cells pre-treated with both a SMYD3i and olaparib were found to be incapable of completely repairing DNA when compared with single drug-treated cells, confirming that combined inhibition impairs DSB repair. Interestingly, the activity of both SMYD3 and PARP1 was also required to efficiently repair endogenous damage (Figure 6A, left panel, and S5C). These results prompted us to evaluate the effect of PARP1 inhibition in wild-type and SMYD3-KO MDA-MB-231 cells. Our data showed that in the absence of SMYD3, BC cells became more sensitive to olaparib (Figure 6B). Moreover, SMYD3-KO cancer cells appeared to have higher levels of basal apoptosis compared with their wild-type counterpart (Figure 6B). To clarify this observation, we analyzed wild-type and SMYD3-KO MDA-MB-231 cells throughout several passages in culture. Our results showed that the SMYD3-KO cells we generated have a limited number of passages; indeed, we observed decreased cell growth and increased cell death after 10–15 passages (Figure S5D). Of note, exogenous re-expression of wild-type SMYD3 in SMYD3-KO MDA-MB-231 cells was able to rescue their phenotype by lowering apoptotic levels (Figure S5E). Finally, to confirm the effect of SMYD3 pharmacological inhibition or genetic ablation observed in BC cells, we analyzed the impact of the SMYD3-R265H mutant on olaparib sensitivity in HEK-293 cells (Low SMYD3, Figure S3A). Although overexpression of wild-type SMYD3 reduced HEK-293 sensitivity to olaparib, the R265H mutant significantly increased apoptosis induction (Figure 6C).

Targeting SMYD3 to Extend the Synthetic Lethality Approach to HR-Proficient Tumors

Based on the above evidence, we hypothesized that combined inhibition of SMYD3 and PARP could represent a valid strategy to induce cancer cell death as a synthetic lethality approach. Specifically, high-SMYD3 and HR-proficient cancer cells might become sensitive to PARP inhibition when combined with SMYD3 inhibition, which impairs HR repair response. Tumors with HR defects are more dependent on PARP to preserve genome integrity (Telli and Ford, 2010). Indeed, inhibition of PARP enzymatic activity directly activates the HR pathway as a way to compensate for the dysfunction; as a consequence, cells with impaired key HR proteins fail to repair DNA damage and restore replication, resulting in cell death (Wang and Weaver, 2011). To get insight into this potential treatment strategy, we treated CRC and BC cells with a SMYD3i and/or olaparib for 72 h and assessed cell death response in single and dual treatment conditions. We found that the combined treatment has a synergistic cytotoxic effect both in MDA-MB-231 and HCT116 cell lines (Figure 6D). We thus extended our analysis to a large panel of BC and CRC cell lines with different mutation profiles and SMYD3 levels (Figure S3A and S5F). Our results confirmed the efficacy of combined SMYD3 and PARP inhibition both in CRC and BC cells with high SMYD3 levels, whereas no significant difference was observed in low-SMYD3 cancer cells (Figure 6E). We further analyzed the biological impact of the combined treatment by characterizing changes in cell fate. Our data revealed that treatment with both a SMYD3i and olaparib promotes apoptosis (Figure 6F). As PARPis are used in the clinics for ovarian and pancreatic BRCA1/2-mutant tumors (Gupta et al., 2019; Zhu et al., 2020; Penson et al., 2020), we further investigated the apoptotic efficacy of the combined treatment in our panel of BC and CRC cells and in OvCa and PC cells with different mutation profiles and SMYD3 levels (Figures S3A and S5F) by annexin V staining (Figures 7A and 7B). Our results confirmed that the combined treatment has a synergistic cytotoxic effect; in particular, PARPi-resistant high-SMYD3 cancer cells are sensitized by SMYD3 inhibition and undergo apoptosis. The high-SMYD3 CAPAN-1 PC cell line was used as a control since it has already been shown to be sensitive to PARP inhibition due to BRCA2 deficiency (McCabe et al., 2005). These data revealed that SMYD3 is synthetic lethal with olaparib in HR-proficient cancer cells, thus extending the potential of the synthetic lethality approach in human tumors.

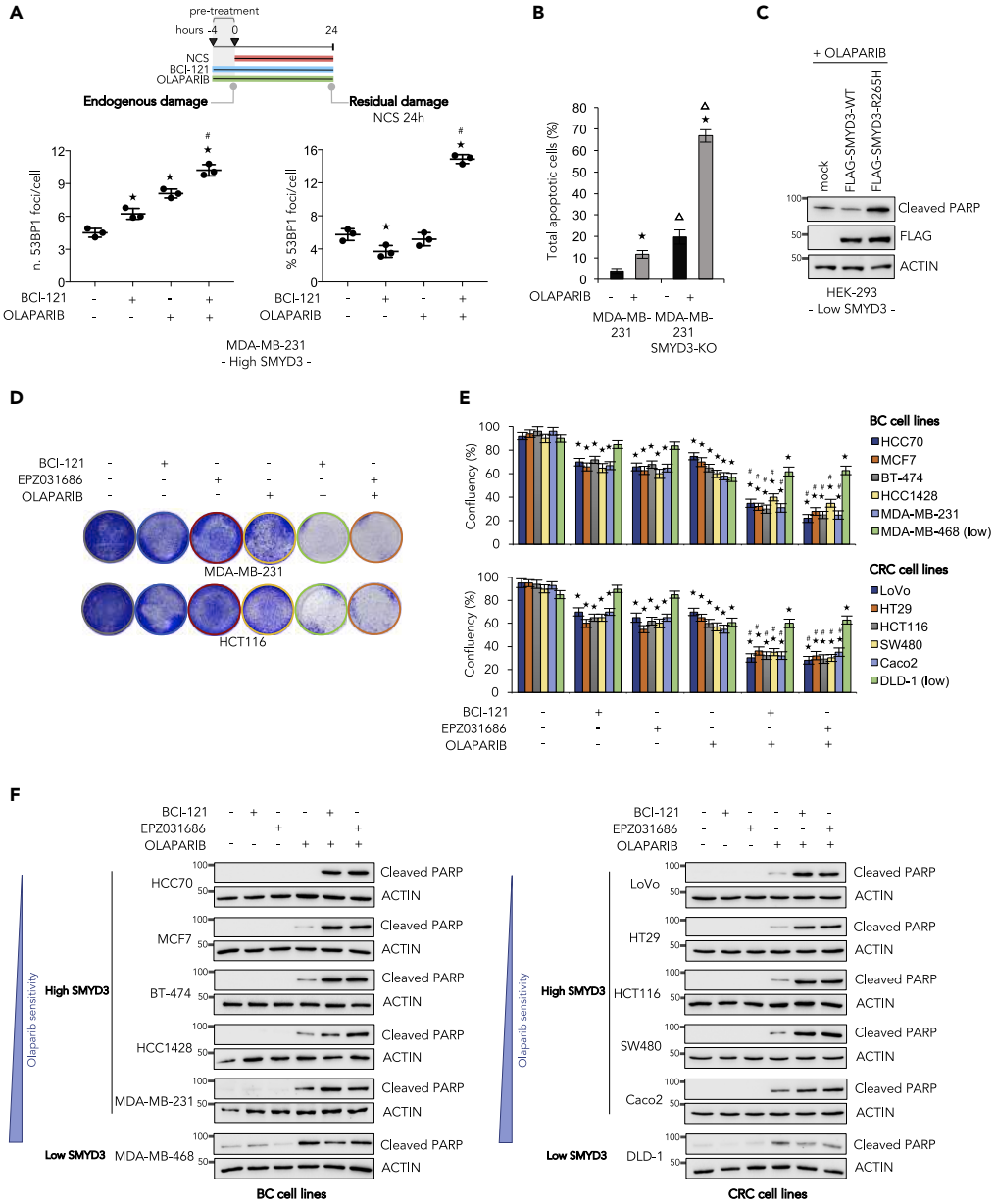

Figure 6. Targeting SMYD3 to Extend the Synthetic Lethality Approach to HR-Proficient Tumors

(A) Upper panel: Treatment scheme. MDA-MB-231 cells were pre-treated for 4 h with BCI-121 (30 μM) and/or olaparib (10 μM), then exposed to NCS (1 nM) for 24 h. Lower panel: Immunostaining with anti-53BP1 antibodies was performed to count nuclear foci. At least 100 cells were analyzed for each time point. The graphs show the number of 53BP1 foci/cell before NCS addition (endogenous damage, left) and the percentage of 53BP1 foci/cell induced by NCS and detectable 24 h after drug exposure (residual damage NCS 24 h, right). Data are presented as mean (SD).

(B) Cell death analysis by annexin V staining. Wild-type and SMYD3-KO MDA-MB-231 cells were treated with olaparib (10 μM) for 72 h and analyzed by flow cytometry for annexin V staining. The indicated percentages of total apoptotic cells include early and late apoptotic and dead cells. Statistical analysis was performed using Student's t-test; ★$p \leq 0.05$, all treatments compared with control; Δ$p \leq 0.05$, SMYD3-KO MDA-MB-231 versus wild-type MDA-MB-231.

(C) Immunoblot analysis showing cleaved PARP levels in HEK-293 cells transfected with FLAG-SMYD3-WT or FLAG-SMYD3-R265H and treated with olaparib for 48 h. FLAG was analyzed as an overexpression control and actin was used as a loading control.

(D) Colony formation assay of MDA-MB-231 and HCT116 cells pre-treated with a SMYD3i (100 μM BCI-121 or 10 μM EPZ031686) for 6 h and then treated with olaparib (10 μM) in the presence of the SMYD3i for a total of 72 h.

Figure 6. *Continued*

(E and F) BC and CRC cell lines were treated as indicated in (D) and cell survival and cell death were assessed by colony formation assay (E) and by immunoblot analysis of cleaved PARP (F), respectively. Actin was used as a loading control. (A and E) ★p ≤ 0.05, all treatments compared with control; #p ≤ 0.05, combined treatments compared with the respective single treatments.

Results are representative of at least three independent experiments. See also Figures S3 and S5.

To evaluate the potential clinical application of SMYD3i/PARPi combined therapy, we determined the fraction of BCs that could be eligible for this therapeutic strategy. To this end, we considered the HR deficiency (HRD) score—which is a biomarker that defines the HRD status and was calculated by Knijnenburg and colleagues by combining scores related to HRD-loss of heterozygosity, large-scale state transitions, and the number of telomeric allelic imbalances—in BCs with high *SMYD3* mRNA expression (Knijnenburg et al., 2018). This analysis revealed that 62.4% (153/245) of BC tumors with high *SMYD3* mRNA levels have a low HRD score (i.e., equal or below the median within the BC dataset) (Figure S4), thus suggesting that 15.6% (153/981) of all analyzed BCs could be eligible for SMYD3i/PARPi combined therapy (high SMYD3/low HRD). Moreover, we determined in the BC dataset the prevalence (Figure S4) and mutual exclusivity of alterations in genes that were previously shown to be significantly associated with a higher HRD score, which means a higher correlation with a homologous recombination deficiency (Figure 8A, Table S2). Alterations with a frequency above 1% were identified in genes (*TP53*, *BRCA1*, *NEIL2*, *HERC2*, *ATM*, *RAD51C*, *BRCA2*, *NSMCE3*, *NUDT15*, *MLH1*, *POLE*, *CHEK1*, *PER1*, *RFC3*, *NEIL3*, *FAAP20*) involved in DDR pathways, including homology-dependent recombination, nucleotide excision repair, and mismatch repair (Knijnenburg et al., 2018) (Figures 3A and S4). Importantly, SMYD3 mRNA overexpression is mutually exclusive with loss-of-function alterations in several genes associated with HRD in cancer, i.e., *TP53*, *BRCA1*, *NEIL2*, *HERC2*, *ATM*, *RAD51C*, and *BRCA2* (Figure 8A and Table S2), supporting the potential of the therapeutic protocol relying on combined SMYD3 and PARP inhibition for HR-proficient tumors with high levels of *SMYD3*.

These results prompted us to evaluate the prevalence and mutual exclusivity of *SMYD3* mRNA overexpression in association with genomic alterations of 43 HRD-associated genes (Knijnenburg et al., 2018), across 459 PanCanAtlas colon and rectum adenocarcinomas (COAD-READ). These tumors were previously analyzed by integrating data on somatic deleterious mutations, deep copy number deletions, and epigenetic silencing events involving a curated list of 276 genes encompassing all major DNA repair pathways (Knijnenburg et al., 2018). This analysis revealed that 126/459 COAD-READ tumors (27%) show *SMYD3* mRNA overexpression and that a low HRD score (i.e., equal or below the median within the COAD-READ dataset) is found in 41.2% of tumors (52/126) with high *SMYD3* mRNA levels (Figure 8B). Furthermore 83% of COAD-READ tumors (383/459) display one or more deleterious alterations in a DNA damage repair gene associated with HRD in cancer, including *MLH1*, *ATM*, *EXO5*, and *HERC2*, which are mutually exclusive with *SMYD3* mRNA overexpression (Figure 8C; Table S2). This analysis suggests that 11% of total CRCs could benefit from SMYD3i/PARPi combined therapy (high SMYD3/low HRD).

Since PARPi therapy has been approved for the treatment of patients with germline or somatic *BRCA1*/*BRCA2*-mutant ovarian and pancreatic cancers, we used TCGA Pan-Cancer ovarian cancer (OV) and pancreatic adenocarcinoma (PAAD) data to evaluate the fraction of patients who could be eligible for SMYD3i/PARPi combined therapy. We included in this analysis a total of 177 OV and 152 PAAD tumors, which were previously characterized for deleterious mutations in DDR genes, to assess the prevalence of HR-proficient and *SMYD3* mRNA-overexpressing tumors. This analysis revealed that 24 of the 51/177 OV tumors with high *SMYD3* mRNA levels and 16 of the 41/152 PAAD tumors with high *SMYD3* mRNA levels have a low HRD score (i.e., equal or below the median within OV and PAAD datasets). Moreover, at least one mutation from a list of 43 HRD-associated genes was detected in 170/177 OV tumors (96%) and 116/152 PAAD tumors (65.3%) (Figure S6). Thus, 13.5% of total OvCas and 10.5% of total PCs could be eligible for SMYD3i/PARPi combined therapy.

Altogether, these results support the potential benefit of combined SMYD3 and PARP inhibition in the management of several solid tumors with HR proficiency and high levels of SMYD3.

DISCUSSION

Personalized medicine is revolutionizing cancer therapy by targeting genes and pathways that are mutated in specific patients' tumors. At present, two different approaches are moving from bench to

A

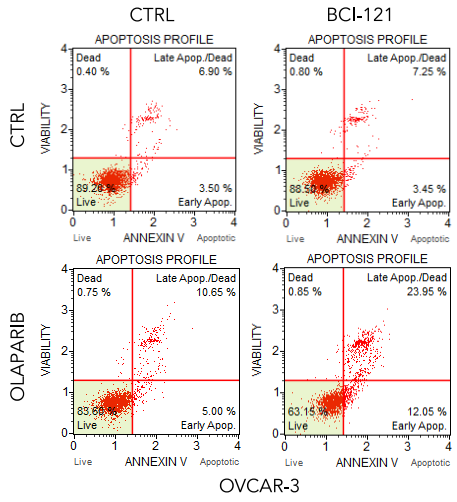

OLAPARIB	BCI-121	Total apoptotic cells (%)
-	-	10,4
-	+	10,7
+	-	15,65
+	+	36

B

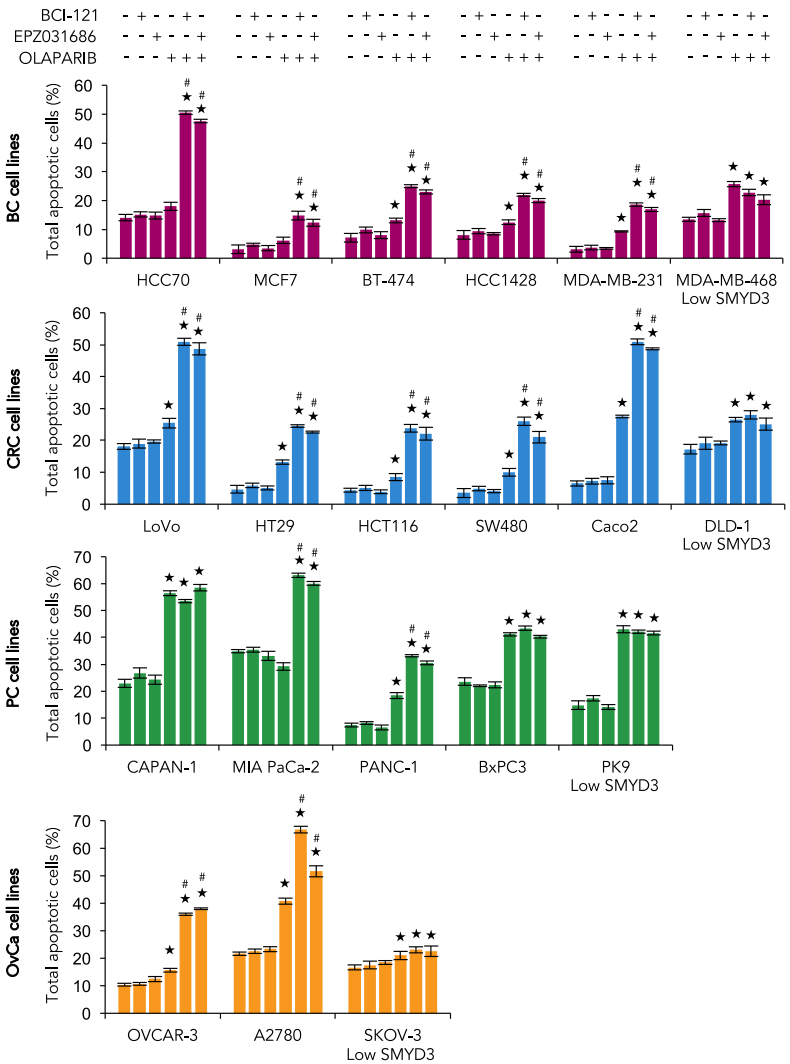

Figure 7. Apoptotic Efficacy of SMYD3i and PARPi Combined Treatment in a Panel of BC, CRC, PC, and OvCa Cell Lines

(A and B) Cell death analysis by annexin V staining. OVCAR-3 (A), BC (red), CRC (blue), PC (green), and OvCa (orange) cell lines (B) were pre-treated with a SMYD3i (100 μM BCI-121 or 10 μM EPZ031686) for 6 h, then treated with olaparib (10 μM) in the presence of the SMYD3i for a total of 72 h and analyzed by flow cytometry for annexin V staining. The indicated percentages of total apoptotic cells include early and late apoptotic and dead cells. Statistical analysis was performed using Student's t-test; ★$p \leq 0.05$, all treatments compared with control; #$p \leq 0.05$, combined treatments compared with the respective single treatments. Results are representative of at least three independent experiments. See also Figure S3.

bedside: oncogene addiction and synthetic lethality. The oncogene addiction approach relies on the observation that tumor cells bearing an activating mutation in a cancer gene are addicted to the signal generated by the encoded gene product and are thus hypersensitive to drugs that specifically target the activated cancer pathway (Weinstein and Joe, 2006). The HER2-targeted antibody trastuzumab used in BC and the VEGF-targeted antibody bevacizumab used in CRC are just a couple of examples (Nahta, 2012; Rosen et al., 2017). Synthetic lethality approaches are based on the assumption that the presence of a mutation in a cancer gene is often associated with a novel vulnerability that can be targeted therapeutically. The genetic principle is that the combination of two genetic perturbations is lethal, whereas each of them individually is not, because the function of the targeted genes is compensatory or partially redundant. Thus, the clinical effect of single drugs individually targeting one of the genes is limited, but their impact is greatly potentiated when they are used in combination (Shen and Ideker, 2018). At present, the only synthetic lethality approach approved in the clinics is based on the use of PARP inhibitors (i.e., olaparib, rucaparib, niraparib, and talazoparib) in BRCA1/2-mutated tumors, as breast, ovarian, and pancreatic cancers.

SMYD3 is a methyltransferase of particular interest for pharmaceutical companies. Indeed, novel inhibitors of this enzyme were recently developed (Fabini et al., 2019a, 2019b; Bottino et al., 2020). However, although its involvement in tumorigenesis is well established—supported by the fact that it is highly overexpressed in several cancers and is required for the development of some types of tumors even in advanced mice models (Sarris et al., 2016)—its role in cancer formation has recently been debated following the publication of a report showing that its genetic ablation or inhibition of its activity does not impair cancer cell autonomous proliferation *in vitro* (Thomenius et al., 2018). This evidence prompted us to undertake an in-depth study of the functional role of SMYD3. A better understanding of SMYD3 function might indeed provide new therapeutic avenues to treat cancer.

As SMYD3 mediates cancer progression by interacting with and regulating key cancer-associated non-histone proteins (Mazur et al., 2014), we performed an *in silico* peptide screening that identified novel SMYD3 interactors, including ATM, CHK2, and BRCA2. These proteins are strictly linked and play important initiator and effector roles in the HR cascade responding to DSBs (Holloman, 2011; Maréchal and Zou, 2013). These data are in agreement with a preliminary study suggesting that SMYD3 is linked to HR repair—although the authors only focused on its gene expression-modulating activity and its effects on long recovery time (Chen et al., 2017)—and with another report hypothesizing that the absence of SMYD3 could arrest cells in the G2/M phase via the ATM-CHK2/p53-Cdc25C pathway (Wang et al., 2017). However, our results clearly support a direct interaction between SMYD3 and ATM. This interaction enables the propagation of a signal cascade through CHK2, which also interacts with SMYD3, by modulating the activity of the third SMYD3 interactor BRCA2, thereby promoting its ability to recruit RAD51 on resected DNA ends. Of note, we found that SMYD3 is a substrate of ATM, and an *in silico* analysis predicted that the targeted amino acid could be residue T268.

This molecular evidence prompted us to study a group of 981 sporadic BCs from the TCGA BC Pan-Cancer dataset. This study revealed that *SMYD3* is altered in 1.2% of all BCs, whereas its mRNA is overexpressed in 25% of them. These data are in agreement with previous reports on cancer tissues (Mazur et al., 2014; Fei et al., 2017) and with an extensive characterization performed on cancer cell lines including BCs and in particular the TNBC phenotype (Peserico et al., 2015 and Figure S3A). Moreover, we found a BC high-risk family carrying a *SMYD3* genetic variant predicted to be deleterious. Intriguingly, the mutation occurs at residue 265, which is located very close to threonine 268, the potential ATM phosphorylation site. This variant correlates with a male and female BC phenotype and was also found in a dataset of patients with CRC (Cerami et al., 2012; Gao et al., 2013). The identification of this variant allowed us to gain further

Figure 8. Analysis of Genomic Alterations and Mutual Exclusivity of SMYD3 and HRD-Associated Genes in PanCanAtlas BC and COAD-READ Datasets

(A) Oncoprint of mutual exclusivity between *SMYD3* mRNA overexpression and deleterious alterations of HRD-associated genes (*TP53, BRCA1, NEIL2, HERC2, ATM, RAD51C,* and *BRCA2*) identified using DISCOVER algorithm at maximum false discover rate (FDR) of 1% across 981 PanCanAtlas BC tumors. BC tumors with somatic alterations in mutually exclusive

Figure 8. *Continued*
genes are depicted in black; BC tumors without somatic alterations in mutually exclusive genes are depicted in gray. Number of BC tumors is indicated below the oncoprint graph (x axis).
(B) Oncoprint of *SMYD3* and HRD-associated genes in PanCanAtlas colon and rectum adenocarcinomas (COAD-READ). Overall profiling of 459 COAD-READ tumors (columns) carrying alterations involving the *SMYD3* gene mRNA overexpression and deleterious mutations, deletions, and epigenetic silencing events for each HRD-associated gene (rows with gene names listed on the left). The association between COAD-READ tumors and the HRD score, low ($\leq$12) and high (>12), is represented as yellow and green bars, respectively. Gray boxes indicate the absence of alterations, and color/shape combinations corresponding to the various alteration types are indicated below the oncoprint. The overall frequency of each gene alteration in the oncoprint plot is indicated on the left.
(C) Oncoprint of mutual exclusivity between *SMYD3* mRNA overexpression and deleterious alterations of HRD-associated genes (*MLH1*, *ATM*, *EXO5*, and *HERC2*) identified using DISCOVER algorithm at maximum false discover rate (FDR) of 1% across 459 PanCanAtlas COAD-READ tumors. COAD-READ tumors with somatic alterations in mutually exclusive genes are depicted in black; COAD-READ tumors without somatic alterations in mutually exclusive genes are depicted in gray. The number of COAD-READ tumors is indicated below the oncoprint graph (x axis).
See also Figures S4 and S6 and Table S2.

molecular clues about SMYD3 protein function in tumors. Our results showed that the R265H mutant protein acts as a dominant negative on ATM, confirming the data obtained by SMYD3 pharmacological inhibition and genetic ablation and unveiling the mechanisms underlying SMYD3 recruitment on DSBs and its active involvement in the repair of DNA lesions.

At the molecular level, we propose that SMYD3 is phosphorylated by ATM and recruited to the site of damaged DNA. At DSB sites, SMYD3 favors the recruitment of various key factors that drive DNA repair through its direct interaction with ATM, BRCA2, and CHK2. Remarkably, the R265H variant identified in the family case study is still capable of associating to DNA break sites but prevents the assembly of a proper DNA repair complex. This suggests that it plays a dominant-negative role, as it displays a very strong interaction with ATM (and phospho-ATM) but loses the ability to interact with BRCA2 and CHK2 to recruit RAD51 to DNA damage sites.

Our findings suggest that SMYD3 plays a role in HR DNA repair also in normal cells. Indeed, the SMYD3 R265H germline mutation was identified in the affected members (two males and one female) of a high-risk BC family. This mutant variant may exert a dominant-negative effect on the wild-type allele by sequestering ATM and preventing proper HR protein complex formation. The analysis of SMYD3 alterations in tumors shows that deleterious mutations have a low frequency, and SMYD3 overexpression, which accounts for around one-third of all cases, is mutually exclusive with mutations occurring in major HR genes. Thus, it seems that these molecular alterations (SMYD3 overexpression and HR gene mutations) may identify two different tumor subsets: one that is HR competent and addicted to SMYD3 overexpression and the other that "classically" displays impairment of major HR genes. Consistently, in our SMYD3-overexpressing cancer cell models, we found that SMYD3 genetic ablation or pharmacological inhibition could trigger a compensatory DNA repair mechanism mediated by PARP1 (Figure 9).

Consistent with a role for SMYD3 in DNA repair, SMYD3 depletion, SMYD3 inhibition, or expression of the R265H variant were all capable, by themselves, to induce endogenous DNA damage accumulation in SMYD3-expressing cancer cells. However, only SMYD3-depleted cells showed a significant defect in rejoining DNA breaks induced by a damaging agent like NCS. Therefore, we hypothesized that activation of one or more compensatory DNA repair signals may occur upon SMYD3 pre-inhibition. Indeed, our experiments highlighted the crucial role of PARP1 in mediating DSB repair in DNA-damaged cells with impaired SMYD3 activity. Thus, we tested the combined treatment with a SMYD3i and a PARPi in order to inhibit both signals, which resulted in cancer cells being incapable of repairing DNA damage. Based on these data, we assessed the efficacy of this combined treatment in BC, CRC, OvCa, and PC cell lines and found that it has a cytotoxic effect and induces apoptotic cell death.

Targeted therapy is currently considered the best approach for fighting cancer. It is based on the use of drugs that specifically interfere with selected molecules involved in cancer development. The increased specificity of this approach allows one to achieve better outcomes and to decrease toxic side effects (Sawyers, 2004). The identification of small-molecule inhibitors that can be associated with PARPis paves the way to new therapeutic protocols and opens up the possibility to extend PARPi/SMYD3i-based treatments even to cancers that are HR proficient and overexpress SMYD3. These represent a significant proportion not only

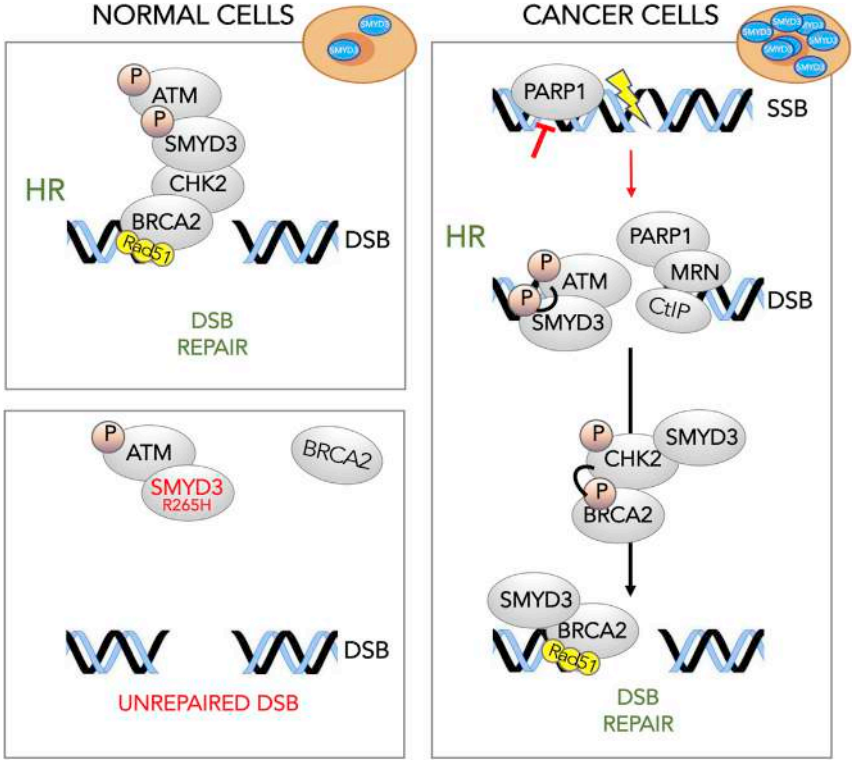

Figure 9. DSB Repair in Depleted/Mutated and Overexpressing SMYD3 Cells

Based on our findings, SMYD3 might play a role in HR DNA repair response in normal cells. Indeed, the presence of the SMYD3 R265H germline mutation may exert a dominant-negative effect on the wild-type allele by sequestering ATM and preventing proper HR protein complex formation. In high SMYD3-expressing cancer cells, phosphorylated SMYD3 by ATM interacts with CHK2 and BRCA2 forming the HR complex required for the final loading of RAD51 at DBS sites. Molecular alterations as SMYD3 overexpression and HR gene mutations may identify two different tumor subsets: one that is HR competent and addicted to SMYD3 overexpression and the other that is influenced by HR gene mutations. In SMYD3-overexpressing cancer cell models, SMYD3 genetic ablation or pharmacological inhibition could trigger a compensatory DNA repair mechanism mediated by PARP1.

of BC (15%) but also of CRC (11%), OvCa (15%), and PC (10%) cases, according to data retrieved from the TCGA Pan-Cancer Atlas.

We believe that our findings, which should be further tested in preclinical cancer models, may provide the basis for future clinical trials to assess the potential of SMYD3 inhibitors in novel therapeutic protocols.

Limitations of the Study

Our results showed that ATM can efficiently phosphoactivate SMYD3 in response to DNA damage, which promotes HR repair; however, we cannot rule out that additional post-translational modifications mediated by and/or affecting SMYD3 activity may be involved in the modulation of HR response. Thus, further investigations are warranted to identify protein modifications that could favor both the assembly of HR multiprotein complexes and RAD51 loading for DSB repair. These would complete the overall molecular picture and may provide novel predictive biomarkers to monitor therapy response. Moreover, our findings would be strengthened by additional testing of the identified synthetic lethality approach in preclinical cancer models, especially *in vivo* systems that mimic human tumors, to further corroborate our findings and devise novel therapeutic strategies for clinical settings. Furthermore, in order to enhance and improve future studies, we have planned to develop more effective and safer SMYD3 inhibitors to translate these findings into clinics.

Resource Availability

Lead Contact

Further information and requests for resources and reagents should be directed to and will be fulfilled by the Lead Contact, Cristiano Simone (cristianosimone73@gmail.com).

Materials Availability

Reagents (peptides, plasmids, and engineered cell lines) generated in this study are available upon request.

Data and Code Availability

In silico data analysis reported in this study were performed as detailed in Transparent Methods section using public repository (i.e., Uniprot, Reactome, cBioPortal), datasets (Colorectal adenocarcinoma, Breast invasive carcinoma, Ovarian serous cystadenocarcinoma, Pancreatic adenocarcinoma of TCGA, PanCancer Atlas), and algorithms (i.e., DISCOVER).

METHODS

All methods can be found in the accompanying Transparent Methods supplemental file.

SUPPLEMENTAL INFORMATION

Supplemental Information can be found online at https://doi.org/10.1016/j.isci.2020.101604.

ACKNOWLEDGMENTS

The authors thank Dr. Francesco Paolo Jori for his helpful discussion during the preparation of the manuscript and editorial assistance, Dr. Vladimir O. Talibov and Prof. Helena Danielson (Department of Chemistry – BMC, Uppsala University, Uppsala, Sweden) for providing the purified SMYD3 protein used in SPR experiments, Valeria Gressani for her technical support, Prof. Ashok Venkitaraman (MRC Cancer Unit, Cambridge, UK) for providing GST-BRCA2 plasmids, Prof. Titia de Lange (The Rockefeller University, New York, USA) for providing GST-ATM plasmids, and Prof. Jeremy Stark (Department of Cancer Genetics and Epigenetics, Beckman Research Institute of the City of Hope, Duarte, California) for providing DR-GFP U2OS cells.

This work was supported by the Fondazione Puglia to P.S., by the Italian Association for Cancer Research (IG grant N. 23794 to C.S., IG grant N.19172 to A.D.R., IG 2018 grant N.21389 to L.O., IG 2018 grant N.21353 to G.C.), by the Italian Ministry of Health "Ricerca Corrente 2018–2020; 2019–2021" to C.S. and "Starting Grant" SG-2019-12371540 to P.S., by the Fondazione Cariplo to G.C., and by the Italian Ministry of Education, University and Research (MIUR) "PRIN - Research Projects of National Relevance" (PRIN 2017, n. 2017WNKSLRLS4) to C.S.

AUTHOR CONTRIBUTIONS

C.S. designed the research and wrote the manuscript; P.S., C.F., and V.D. performed the biological and computational assays, analyzed and reviewed the data, and collaborated to write the manuscript; G.B. performed the experiments and reviewed the data and the manuscript for important intellectual content; C.B., S.C., E.F., V.S., V.V., G.F., M.L.S., K.D.M., S.B., U.G., N.P., V.D.M., and E.M. conducted the biological assays; V.G. and M.B. coordinated the experimental work and reviewed the data; G.G. reviewed the manuscript for important intellectual content; A.D.R., G.C., and L.O. collaborated to design the study and write the manuscript.

DECLARATION OF INTERESTS

The authors declare no competing interests.

Received: May 4, 2020
Revised: August 7, 2020
Accepted: September 21, 2020
Published: October 23, 2020

REFERENCES

Apostolou, P., and Papasotiriou, I. (2017). Current perspectives on CHEK2 mutations in breast cancer. Breast Cancer *9*, 331–335.

Bakkenist, C.J., and Kastan, M.B. (2003). DNA damage activates ATM through intermolecular autophosphorylation and dimer dissociation. Nature *421*, 499–506.

Bottino, C., Peserico, A., Simone, C., and Caretti, G. (2020). SMYD3: an oncogenic driver targeting epigenetic regulation and signaling pathways. Cancers (Basel) *12*, E142.

Brown, M.A., Foreman, K., Harriss, J., Chhaya, D., Zhu, L., Edwards, M., Shaaban, S., and Tucker, H. (2015). C-terminal domain of SMYD3 serves as a unique HSP90-regulated motif in oncogenesis. Oncotarget *6*, 4005–4019.

Buchtel, K.M., Vogel Postula, K.J., Weiss, S., Williams, C., Pineda, M., and Weissman, S.M. (2018). FDA approval of PARP inhibitors and the impact on genetic counseling and genetic testing practices. J. Genet. Couns. *27*, 131–139.

Carreira, A., Hilario, J., Amitani, I., Baskin, R.J., Shivji, M.K.K., Venkitaraman, A.R., and Kowalczykowski, S.C. (2009). The BRC repeats of BRCA2 modulate the DNA-binding selectivity of RAD51. Cell *136*, 1032–1043.

Cerami, E., Gao, J., Dogrusoz, U., Gross, B.E., Sumer, S.O., Aksoy, B.A., Jacobsen, A., Byrne, C.J., Heuer, M.L., Larsson, E., et al. (2012). The cBio cancer genomics portal: an open platform for exploring multidimensional cancer genomics data. Cancer Discov. *2*, 401–404.

Chatterjee, G., Jimenez-Sainz, J., Presti, T., Nguyen, T., and Jensen, R.B. (2016). Distinct binding of BRCA2 BRC repeats to RAD51 generates differential DNA damage sensitivity. Nucleic Acids Res. *44*, 5256–5270.

Chen, Y.J., Tsai, C.H., Wang, P.Y., and Teng, S.C. (2017). SMYD3 promotes homologous recombination via regulation of H3K4-mediated gene expression. Sci. Rep. *7*, 3842.

Cock-Rada, A.M., Medjkane, S., Janski, N., Yousfi, N., Perichon, M., Chaussepied, M., Chluba, J., Langsley, G., and Weitzman, J.B. (2012). SMYD3 promotes cancer invasion by epigenetic upregulation of the metalloproteinase MMP-9. Cancer Res. *72*, 810–820.

Dedon, P.C., and Goldberg, I.H. (1992). Free-radical mechanisms involved in the formation of sequence- dependent bistranded DNA lesions by the antitumor antibiotics bleomycin, neocarzinostatin, and calicheamicin. Chem. Res. Toxicol. *5*, 311–332.

Fabini, E., Manoni, E., Ferroni, C., Del Rio, A., and Bartolini, M. (2019a). Small-molecule inhibitors of lysine methyltransferases SMYD2 and SMYD3: current trends. Future Med. Chem. *11*, 901–921.

Fabini, E., Talibov, V.O., Mihalic, F., Naldi, M., Bartolini, M., Bertucci, C., Del Rio, A., and Danielson, U.H. (2019b). Unveiling the biochemistry of the epigenetic regulator SMYD3. Biochemistry *58*, 3634–3645.

Falck, J., Coates, J., and Jackson, S.P. (2005). Conserved modes of recruitment of ATM, ATR and DNA-PKcs to sites of DNA damage. Nature *434*, 605–611.

Fei, X., Ma, Y., Liu, X., and Meng, Z. (2017). Overexpression of SMYD3 is predictive of unfavorable prognosis in hepatocellular carcinoma. Tohoku J. Exp. Med. *243*, 219–226.

Fenizia, C., Bottino, C., Corbetta, S., Fittipaldi, R., Floris, P., Gaudenzi, G., Carra, S., Cotelli, F., Vitale, G., Caretti, G., et al. (2019). SMYD3 promotes the epithelial-mesenchymal transition in breast cancer. Nucleic Acids Res. *47*, 1278–1293.

Gao, J., Aksoy, B.A., Dogrusoz, U., Dresdner, G., Gross, B., Sumer, S.O., Sun, Y., Jacobsen, A., Sinha, R., Larsson, E., et al. (2013). Integrative analysis of complex cancer genomics and clinical profiles using the cBioPortal. Sci. Signal. *6*, pl1.

Gunn, A., and Stark, J.M. (2012). I-SceI-based assays to examine distinct repair outcomes of mammalian chromosomal double strand breaks. Methods Mol. Biol. *920*, 379–391.

Gupta, M., Iyer, R., and Fountzilas, C. (2019). Poly(ADP-Ribose) polymerase inhibitors in pancreatic cancer: a new treatment paradigms and future implications. Cancers (Basel) *11*, 1980.

Hamamoto, R., Furukawa, Y., Masashi, M., Iimura, Y., Pittella Silva, F., Li, M., Yagyu, R., and Nakamura, Y. (2004). SMYD3 encodes a histone methyltransferase involved in the proliferation of cancer cells. Nat. Cell Biol. *6*, 731–740.

Hamamoto, R., Pittella Silva, F., Tsuge, M., Toshihiko Nishidate, T., Katagiri, T., Nakamura, Y., and Furukawa, Y. (2006). Enhanced SMYD3 expression is essential for the growth of breast cancer cells. Cancer Sci. *97*, 113–118.

Holloman, W.K. (2011). Unraveling the mechanism of BRCA2 in homologous recombination. Nat. Struct. Mol. Biol. *18*, 748–754.

Jeon, O.H., Kim, D., and Choi, J. (2007). Novel function of human ADAM15 disintegrin-like domain and its derivatives in platelet aggregation. Thromb. Res *119*, 609–619.

Jerzak, K.J., Mancuso, T., and Eisen, A. (2018). Ataxia-telangiectasia gene (ATM) mutation heterozygosity in breast cancer: a narrative review. Curr. Oncol. *25*, e176–e180.

Kanduc, D. (2010). Protein information content resides in rare peptide segments. Peptides *31*, 983–988.

Kataya, A., Schei, E., and Lillo, C. (2015). MAP kinase phosphatase 1 harbors a novel PTS1 and is targeted to peroxisomes following stress treatments. J. Plant Physiol. *179*, 12–20.

Kieken, F., Jović, M., Tonelli, M., Naslavsky, N., Caplan, S., and Sorgen, P.L. (2009). Structural insight into the interaction of proteins containing NPF, DPF, and GPF motifs with the C-terminal EH-domain of EHD1. Protein Sci. *18*, 2471–2479.

Kim, H., Heo, K., Kim, J.H., Kim, K., Choi, J., and An, W. (2009). Requirement of histone methyltransferase SMYD3 for estrogen receptor-mediated transcription. J. Biol. Chem. *284*, 19867–19877.

Kim, J.M., Kim, K., Schmidt, T., Punj, V., Tucker, H., Rice, J.C., Ulmer, T.S., and An, W. (2015). Cooperation between SMYD3 and PC4 drives a distinct transcriptional program in cancer cells. Nucleic Acids Res. *43*, 8868–8883.

Knijnenburg, T.A., Wang, L., Zimmermann, M.T., Chambwe, N., Gao, G.F., Cherniack, A.D., Fan, H., Shen, H., Way, G.P., Greene, C.S., et al. (2018). Genomic and molecular landscape of DNA damage repair deficiency across the cancer genome atlas. Cell Rep. *23*, 239–254.e6.

Krejci, L., Altmannova, V., Spirek, M., and Zhao, X. (2012). Homologous recombination and its regulation. Nucleic Acids Res. *40*, 5795–5818.

Kunizaki, M., Hamamoto, R., Fabio Pittella Silva, F., Yamaguchi, K., Nagayasu, T., Shibuya, M., Nakamura, Y., and Furukawa, Y. (2007). The lysine 831 of vascular endothelial growth factor receptor 1 is a novel target of methylation by SMYD3. Cancer Res. *67*, 10759–10765.

Kusalik, A., Trost, B., Bickis, M., Fasano, C., Capone, G., and Kanduc, D. (2009). Codon number shapes peptide redundancy in the universal proteome composition. Peptides *30*, 1940–1944.

Lee, J.H., and Paull, T.T. (2007). Activation and regulation of ATM kinase activity in response to DNA double-strand breaks. Oncogene *26*, 7741–7748.

Lee, M., Daniels, M.J., and Venkitaraman, A.R. (2004). Phosphorylation of BRCA2 by the polo-like kinase Plk1 is regulated by DNA damage and mitotic progression. Oncogene *23*, 865–872.

Luo, X.G., Zhang, C.L., Zhao, W.W., Liu, Z.P., Liu, L., Mu, A., Guo, S., Wang, N., Zhou, H., and Zhang, T.C. (2014). Histone methyltransferase SMYD3 promotes MRTF-A-mediated transactivation of MYL9 and migration of MCF-7 breast cancer cells. Cancer Lett. *344*, 129–137.

Maréchal, A., and Zou, L. (2013). DNA damage sensing by the ATM and ATR kinases. Cold Spring Harb. Perspect. Biol. *5*, a012716.

Mazur, P.K., Reynoird, N., Khatri, P., Jansen, P.W.T.C., Wilkinson, A.W., Liu, S., Barbash, O., Van Aller, G.S., Huddleston, M., Dhanak, D., et al. (2014). SMYD3 links lysine methylation of MAP3K2 to Ras-driven cancer. Nature *510*, 283–287.

McCabe, N., Lord, C.J., Tutt, A.N.J., Martin, N., Smith, G.C.M., and Ashworth, A. (2005). BRCA2-deficient CAPAN-1 cells are extremely sensitive to the inhibition of poly (ADP-ribose) polymerase: an issue of potency. Cancer Biol. Ther. *4*, 934–936.

Nahta, R. (2012). Molecular mechanisms of trastuzumab-based treatment in HER2-overexpressing breast cancer. ISRN Oncol. *2012*, 428062.

Nam, A.S., Yin, Y., von Marschall, Z., and Fisher, L.W. (2014). Efficient trafficking of acidic proteins out of the endoplasmic reticulum involves a conserved amino terminal IleProVal (IPV)-like

tripeptide motif. Connect. Tissue Res. *55*, 138–141.

Nishimura, A., and Linder, M.E. (2013). Identification of a novel prenyl and palmitoyl modification at the caax motif of cdc42 that regulates RhoGDI binding. Mol. Cell Biol. *33*, 1417–1429.

Panier, S., and Boulton, S.J. (2014). Double-strand break repair: 53BP1 comes into focus. Nat. Rev. Mol. Cell Biol. *15*, 7–18.

Pascal, J.M. (2018). The comings and goings of PARP-1 in response to DNA damage. DNA Repair (Amst) *71*, 177–182.

Penson, R.T., Valencia, R.V., Cibula, D., Colombo, N., Leath, C.A., Bidziński, M., Kim, J.W., Nam, J.H., Madry, R., Hernández, C., et al. (2020). Olaparib versus nonplatinum chemotherapy in patients with platinum-sensitive relapsed ovarian cancer and a germline BRCA1/2 mutation (SOLO3): a randomized phase III trial. J. Clin. Oncol. *38*, 1164–1174.

Peserico, A., Germani, A., Sanese, P., Barbosa, A.J., Di Virgilio, V., Fittipaldi, R., Fabini, E., Bertucci, C., Varchi, G., Pat Moyer, M., et al. (2015). A SMYD3 small-molecule inhibitor impairing cancer cell growth. J. Cell. Physiol. *230*, 2447–2460.

Petrucelli, N., Daly, M.B., and Feldman, G.L. (2010). Hereditary breast and ovarian cancer due to mutations in BRCA1 and BRCA2. Genet. Med. *12*, 245–259.

Pierce, A.J., Johnson, R.D., Thompson, L.H., and Jasin, M. (1999). XRCC3 promotes homology-directed repair of DNA damage in mammalian cells. Genes Dev. *13*, 2633–2638.

Proserpio, V., Fittipaldi, R., Ryall, J.G., Sartorelli, V., and Caretti, G. (2013). The methyltransferase SMYD3 mediates the recruitment of transcriptional cofactors at the myostatin and c-Met genes and regulates skeletal muscle atrophy. Genes Dev. *27*, 1299–1312.

Reiss, D.J., and Schwikowski, B. (2004). Predicting protein-peptide interactions via a network-based motif sampler. Bioinformatics *20*, i274–i282.

Rizzolo, P., Zelli, V., Valentina Silvestri, V., Virginia Valentini, V., Zanna, I., Bianchi, S., Masala, G., Spinelli, A.M., Tibiletti, M.G., Russo, A., et al. (2019). Insight into genetic susceptibility to male breast cancer by multigene panel testing: results from a multicenter study in Italy. Int. J. Cancer *145*, 390–400.

Rosen, L.S., Jacobs, I.A., and Burkes, R.L. (2017). Bevacizumab in colorectal cancer: current role in treatment and the potential of biosimilars. Target Oncol. *12*, 599–610.

Sarris, M.E., Moulos, P., Haroniti, A., Giakountis, A., and Talianidis, I. (2016). Smyd3 is a transcriptional potentiator of multiple cancer-promoting genes and required for liver and colon cancer development. Cancer Cell *29*, 354–366.

Sawyers, C. (2004). Targeted cancer therapy. Nature *432*, 294–297.

Shen, J.P., and Ideker, T. (2018). Synthetic lethal networks for precision oncology: promises and pitfalls. J. Mol. Biol. *430*, 2900–2912.

Shiloh, Y. (2003). ATM and related protein kinases: safeguarding genome integrity. Nat. Rev. Cancer *3*, 155–168.

Sudnitsyna, M.V., Mymrikov, E.V., Seit-Nebi, A.S., and Gusev, N.B. (2012). The role of intrinsically disordered regions in the structure and functioning of small heat shock proteins. Curr. Protein Pept. Sci. *13*, 76–85.

Sun, Y., McCorvie, T.J., Yates, L.A., and Zhang, X. (2020). Structural basis of homologous recombination. Cell. Mol. Life Sci. *77*, 3–18.

Takai, H., Wang, R.C., Takai, K.K., Yang, H., and de Lange, T. (2007). Tel2 regulates the stability of PI3K-related protein kinases. Cell *131*, 1248–1259.

Tazzite, A., Jouhadi, H., Benider, A., and Nadifi, S. (2020). BRCA mutational status is a promising predictive biomarker for platinum-based chemotherapy in triple-negative breast. Curr. Drug Targets. https://doi.org/10.2174/1389450121666200203162541.

Telli, M.L., and Ford, J.M. (2010). PARP inhibitors in breast cancer. Clin. Adv. Hematol. Oncol. *8*, 629–635.

Thomenius, M.J., Totman, J., Harvey, D., Mitchell, L.H., Riera, T.V., Cosmopoulos, K., Grassian, A.R., Klaus, C., Foley, M., Admirand, E.A., et al. (2018). Small molecule inhibitors and CRISPR/Cas9 mutagenesis demonstrate that SMYD2 and SMYD3 activity are dispensable for autonomous cancer cell proliferation. PLoS One *13*, e0197372.

Tsuge, M., Hamamoto, R., Pittella Silva, F., Ohnishi, Y., Chayama, K., Kamatani, N., Furukawa, Y., and Nakamura, Y. (2005). A variable number of tandem repeats polymorphism in an E2F-1 binding element in the 5′ flanking region of SMYD3 is a risk factor for human cancers. Nat. Genet. *37*, 1104.

UniProt Consortium (2014). UniProt: a hub for protein information. Nucleic Acids Res. *43*, D204–D212.

Wang, L., Wang, Q.T., Liu, Y.P., Dong, Q.Q., Hu, H.J., Miao, Z., Li, S., Liu, Y., Zhou, H., Zhang, T.C., et al. (2017). ATM signaling pathway is implicated in the SMYD3-mediated proliferation and migration of gastric cancer cells. J. Gastric Cancer *17*, 295–305.

Wang, X., and Weaver, D.T. (2011). The ups and downs of DNA repair biomarkers for PARP inhibitor therapies. Am. J. Cancer Res. *1*, 301–327.

Weinstein, I.B., and Joe, A.K. (2006). Mechanisms of disease: oncogene addiction-a rationale for molecular targeting in cancer therapy. Nat. Clin. Pract. Oncol. *3*, 448–457.

Wong, S.S., Østergaard, S., Hall, G., Li, C., Williams, P.M., Stennicke, H., and Emsley, J. (2016). A novel DFP tripeptide motif interacts with the coagulation factor XI apple 2 domain. Blood *127*, 2915–2923.

Yoshioka, Y., Suzuki, T., Matsuo, Y., Tsurita, G., Watanabe, T., Dohmae, N., Nakamura, Y., and Hamamoto, R. (2017). Protein lysine methyltransferase SMYD3 is involved in tumorigenesis through regulation of HER2 homodimerization. Cancer Med. *6*, 1665–1672.

Yoshioka, Y., Suzuki, T., Matsuo, Y., Nakakido, M., Tsurita, G., Simone, C., Watanabe, T., Dohmae, N., Nakamura, Y., and Hamamoto, R. (2016). SMYD3-mediated lysine methylation in the PH domain is critical for activation of AKT1. Oncotarget *7*, 75023–75037.

You, Z., Bailis, J.M., Johnson, S.A., Dilworth, S.M., and Hunter, T. (2007). Rapid activation of ATM on DNA flanking double-strand breaks. Nat. Cell Biol. *9*, 1311–1318.

Zhu, C.L., and Huang, Q. (2020). Overexpression of the SMYD3 promotes proliferation, migration, and invasion of pancreatic cancer. Dig. Dis. Sci. *65*, 489–499.

Zhu, H., Wei, M., Xu, J., Hua, J., Liang, C., Meng, Q., Zhang, Y., Liu, J., Zhang, B., Yu, X., et al. (2020). PARP inhibitors in pancreatic cancer: molecular mechanisms and clinical applications. Mol. Cancer *19*, 49.

Zou, J.N., Wang, S.Z., Yang, J.S., Luo, X.G., Xie, J.H., and Xi, T. (2009). Knockdown of SMYD3 by RNA interference down-regulates c-Met expression and inhibits cells migration and invasion induced by HGF. Cancer Lett. *280*, 78–85.

iScience, Volume *23*

Supplemental Information

Targeting SMYD3 to Sensitize Homologous Recombination-Proficient Tumors to PARP-Mediated Synthetic Lethality

Paola Sanese, Candida Fasano, Giacomo Buscemi, Cinzia Bottino, Silvia Corbetta, Edoardo Fabini, Valentina Silvestri, Virginia Valentini, Vittoria Disciglio, Giovanna Forte, Martina Lepore Signorile, Katia De Marco, Stefania Bertora, Valentina Grossi, Ummu Guven, Natale Porta, Valeria Di Maio, Elisabetta Manoni, Gianluigi Giannelli, Manuela Bartolini, Alberto Del Rio, Giuseppina Caretti, Laura Ottini, and Cristiano Simone

Compound	Amino acid sequence	Molecular weight (Da)
P1	NFF	440,5
P2	DFF	441,5
P3	LFF	439,6
P4	FFF	473,6
P5	QFF	454,5
P6	KFF	454,6
P7	NIF	406,5
P8	NYF	456,5
P9	NAF	364,4
P10	NDF	408,4
P11	NHF	430,5
P12	NNF	407,4
P13	NFI	406,5
P14	NFY	456,5
P15	NFA	364,5
P16	NFH	430,5
P17	NFW	479,5
P18	NFR	449,5
P19	NFK	421,5

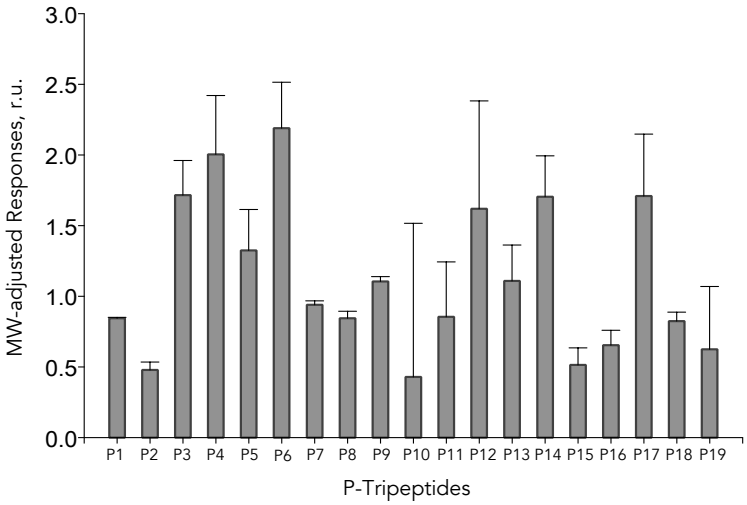

Figure S1. SPR analysis of selected P-tripeptides interaction with SMYD3, (Related to Figure 1).
Left: List of P-tripeptides with their amino acid composition and molecular weight. Right: Histogram of MW-adjusted SPR responses for the tested P-tripeptides. Shown double-referenced responses refer to the SAM-free assay. No difference in binding responses between SAM-free and SAM-saturated binding events emerged, suggesting no allosteric effect.

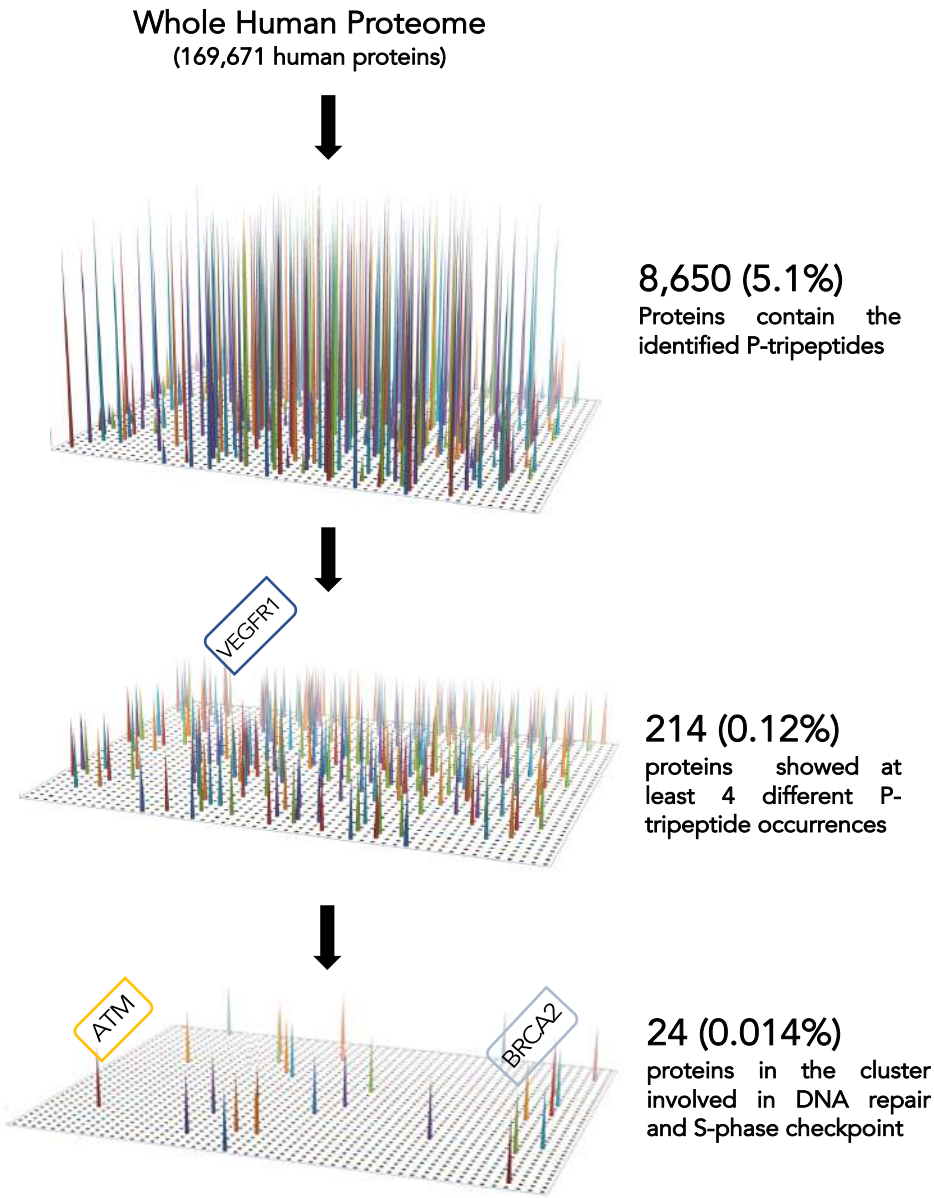

Figure S2. Procedural scheme of P-tripeptide screening in the human proteome, (Related to Figure 1). The exact distribution of each P-tripeptide in all human proteins annotated in the UniProt/SwissProt database (analysis performed in December 2018; https://www.uniprot.org) was analyzed using the Peptide search tool (https://www.uniprot.org/peptidesearch/). The entire human proteome was scanned to search for exact matches of each P-tripeptide. Among 8,650 proteins containing the identified tripeptides, only 214 showed at least 4 different tripeptide occurrences. These 214 proteins represented our starting subset to analyze potential candidates as new SMYD3 interactors. Next, we clustered these 214 proteins based on their biological function annotated in the corresponding Uniprot entry and confirmed the clustering in the Reactome database (e.g. HR pathway, Reactome id: R-HSA- 5685942; http://reactome.org). In the subset of 214 proteins showing at least 4 different tripeptide occurrences, we observed an enrichment in factors (24 proteins) involved in DNA repair and S- phase checkpoint (e.g. ATM, BRCA2).

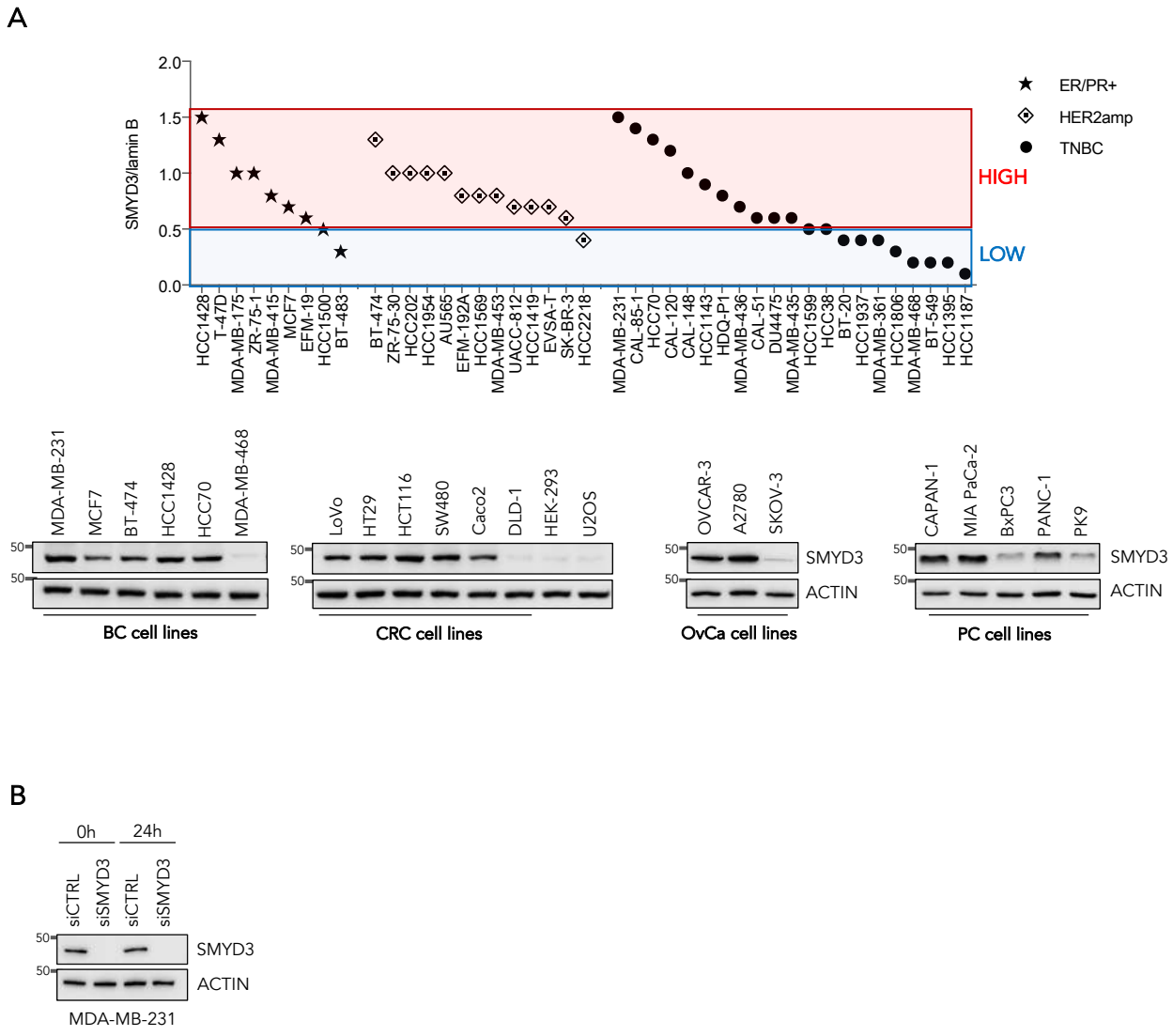

Figure S3. Analysis of SMYD3 protein levels in BC cell lines (Related to Figures 2, 4, 5, 6, 7).
(A) Upper panel: Densitometric analysis of SMYD3 levels, normalized against the loading control, in 43 BC cell lines classified for estrogen (ER) or progesterone (PR) receptor positivity and human epidermal growth factor receptor 2 (HER2) status; TNBC: triple-negative breast cancer cell lines without any marker positivity. Lower panel: immunoblotting analysis of SMYD3 protein levels in all the cell lines used in this study.
(B) Immunoblotting analysis of SMYD3 protein levels in MDA-MB-231 cells transfected with siCTRL and siSMYD3 depicted in Figure 2A. Actin was used as a loading control.

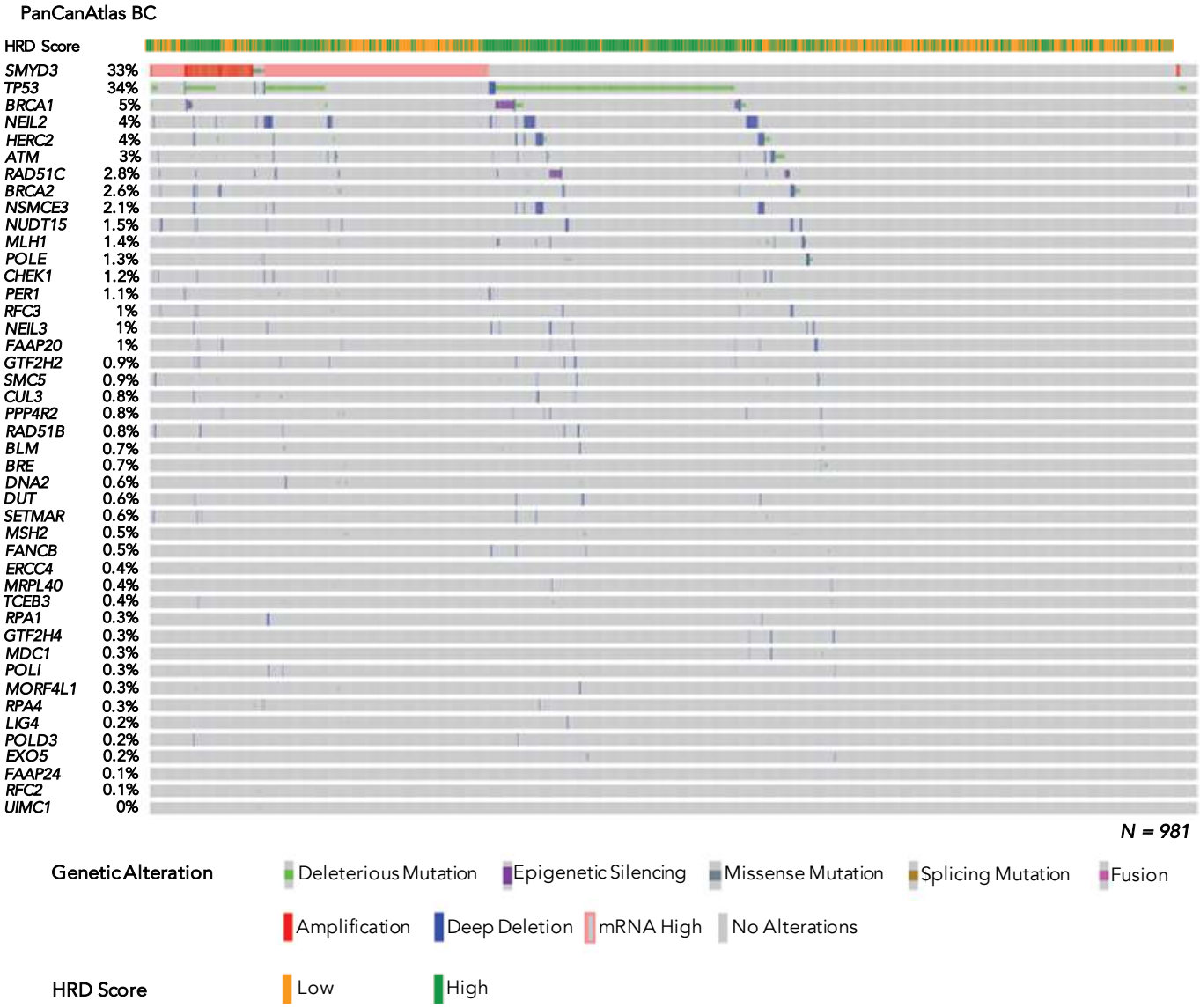

Figure S4. Oncoprint of SMYD3 and HRD-associated genes in PanCanAtlas BC tumors, (Related to Figures 3, 8).

Overall profiling of 981 BC tumors (columns) carrying alterations involving the SMYD3 gene (mRNA overexpression (25%), copy number alterations (6.7%), and mutations (1.12%) and deleterious mutations, deletions, and epigenetic silencing events for each HRD-associated gene (rows with gene names listed on the left). The association between BC tumors and the HRD score, low (≤ 21) and high (> 21), is represented as yellow and green bars, respectively. Grey boxes indicate the absence of alterations, and color/shape combinations corresponding to the various alteration types are indicated below the oncoprint. The frequency of each gene alteration in the oncoprint plot is indicated on the left.

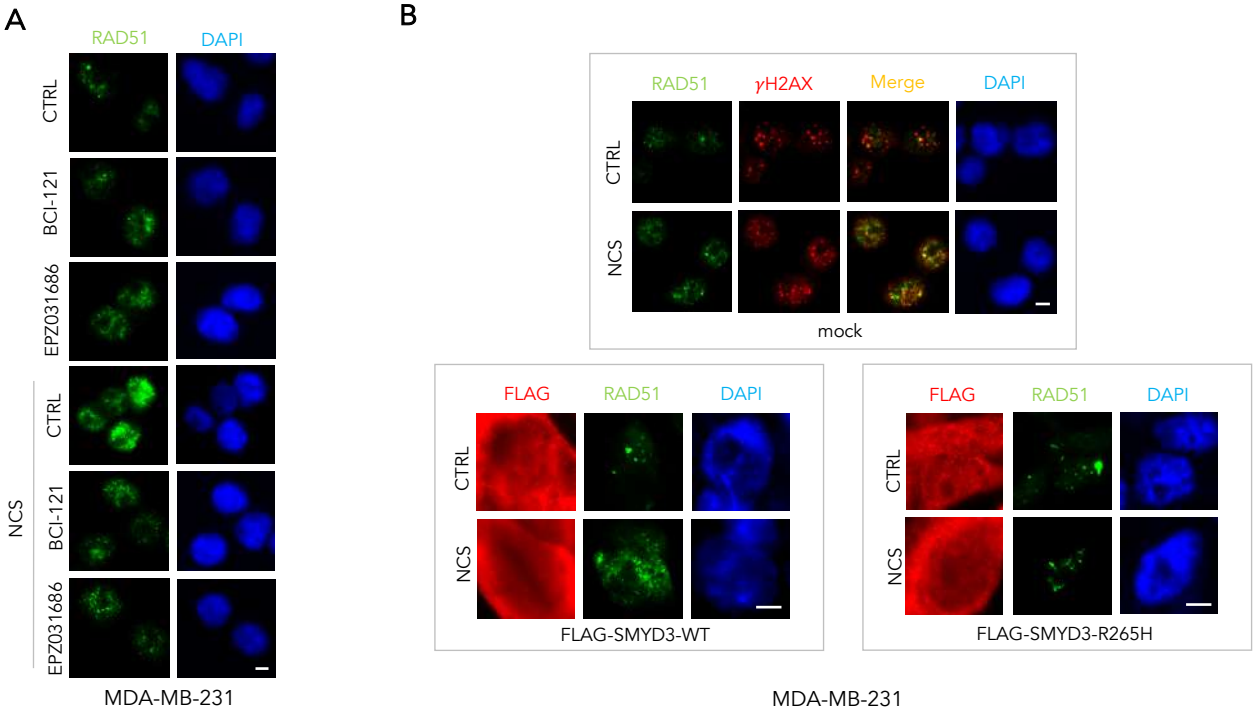
A
RAD51
DAPI
CTRL
BCI-121
EPZ031686
NCS
CTRL
BCI-121
EPZ031686
MDA-MB-231
B
RAD51
γH2AX
Merge
DAPI
CTRL
NCS
mock
FLAG
RAD51
DAPI
CTRL
NCS
FLAG-SMYD3-WT
FLAG-SMYD3-R265H
MDA-MB-231

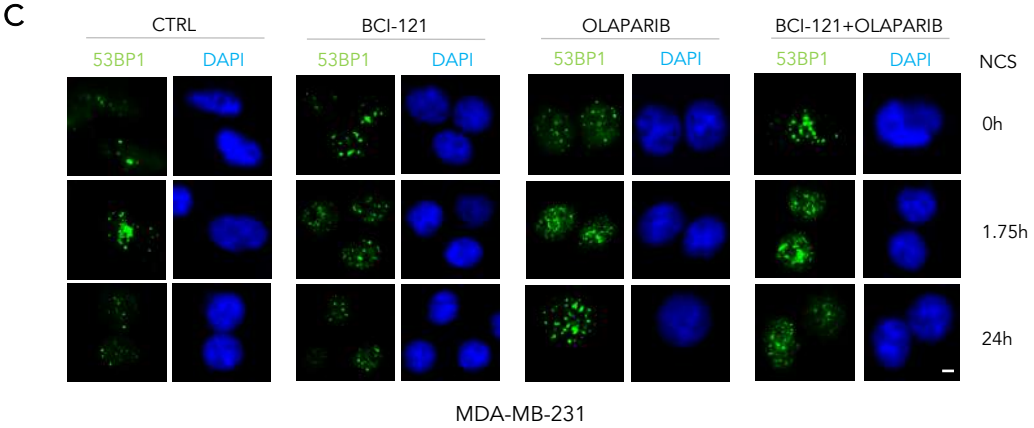
C
CTRL
BCI-121
OLAPARIB
BCI-121+OLAPARIB
53BP1
DAPI
NCS
0h
1.75h
24h
MDA-MB-231

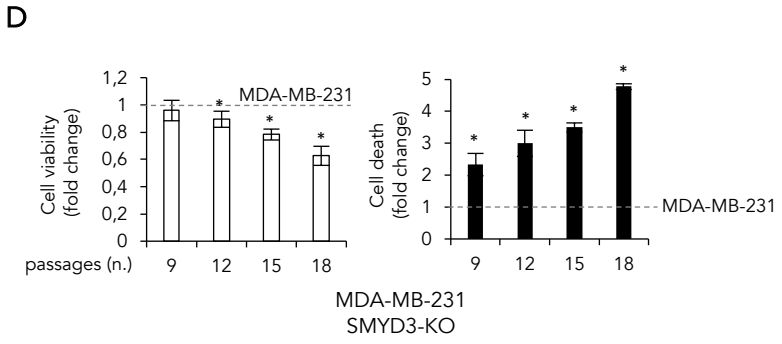
D
Cell viability (fold change)
MDA-MB-231
passages (n.)
9
12
15
18
Cell death (fold change)
MDA-MB-231
MDA-MB-231
SMYD3-KO

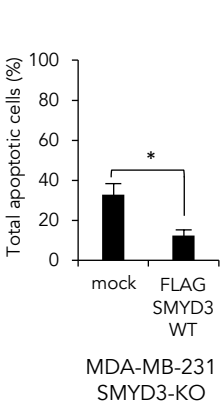
E
Total apoptotic cells (%)
mock
FLAG SMYD3 WT
MDA-MB-231
SMYD3-KO

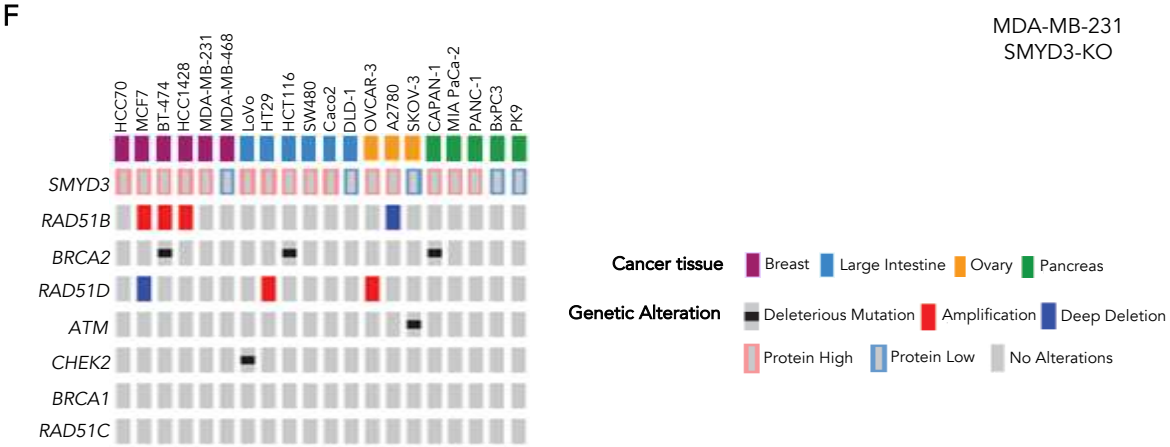
F
HCC70
MCF7
BT-474
HCC1428
MDA-MB-231
MDA-MB-468
LoVo
HT29
HCT116
SW480
Caco2
DLD-1
OVCAR-3
A2780
SKOV-3
CAPAN-1
MIA PaCa-2
PANC-1
BxPC3
PK9
SMYD3
RAD51B
BRCA2
RAD51D
ATM
CHEK2
BRCA1
RAD51C
Cancer tissue
Breast
Large Intestine
Ovary
Pancreas
Genetic Alteration
Deleterious Mutation
Amplification
Deep Deletion
Protein High
Protein Low
No Alterations

Figure S5. Characterization of SMYD3 role in DSB repair and mutation profiling in cancer cells, (Related to Figures 1, 5, 6, 7).

(A) Immunostaining for RAD51 (green) in MDA-MB-231 cells pre-treated for 4 h with BCI-121 (30 μM) or EPZ031686 (1 μM) and then subjected to DNA damage with NCS (1 nM) for 6 h. Nuclei were stained with DAPI (blue).

(B) Immunostaining of MDA-MB-231 cells treated with NCS (1 μM) for 6 h. Left panel: Immunostaining for RAD51 (green) and γH2AX (red) in untransfected MDA-MB-231 cells. Right panel: Immunostaining for RAD51 (green) and FLAG (red) in MDA-MB-231 cells transfected with FLAG-SMYD3-WT or FLAG-SMYD3-R265H. Nuclei were stained with DAPI (blue).

(C) Immunostaining for 53BP1 (green) in MDA-MB-231 cells pre-treated for 4 h with BCI-121 (30 μM) and/or olaparib (10 μM) and then exposed to NCS (1 nM) for 24 h. Nuclei were stained with DAPI (blue). (A,B,C) The scale bar represents 5 μm.

(D) Quantification of cell viability and cell death by trypan blue staining in SMYD3-KO MDA-MB-231 cells at the indicated culture passages, normalized against wild-type MDA-MB-231 cells.

(E) Cell death analysis by annexin V staining. SMYD3-KO MDA-MB-231 cells were transfected with FLAG-SMYD3-WT for 24 h and then analyzed by flow cytometry for annexin V staining. The indicated percentages of total apoptotic cells include early and late apoptotic and dead cells.

(D, E) Statistical analysis was performed using Student's t-test; $*p \leq 0.05$. Results are representative of at least three independent experiments.

(F) Mutation profiles of selected BC, CRC, OvCa, and PC cell lines.

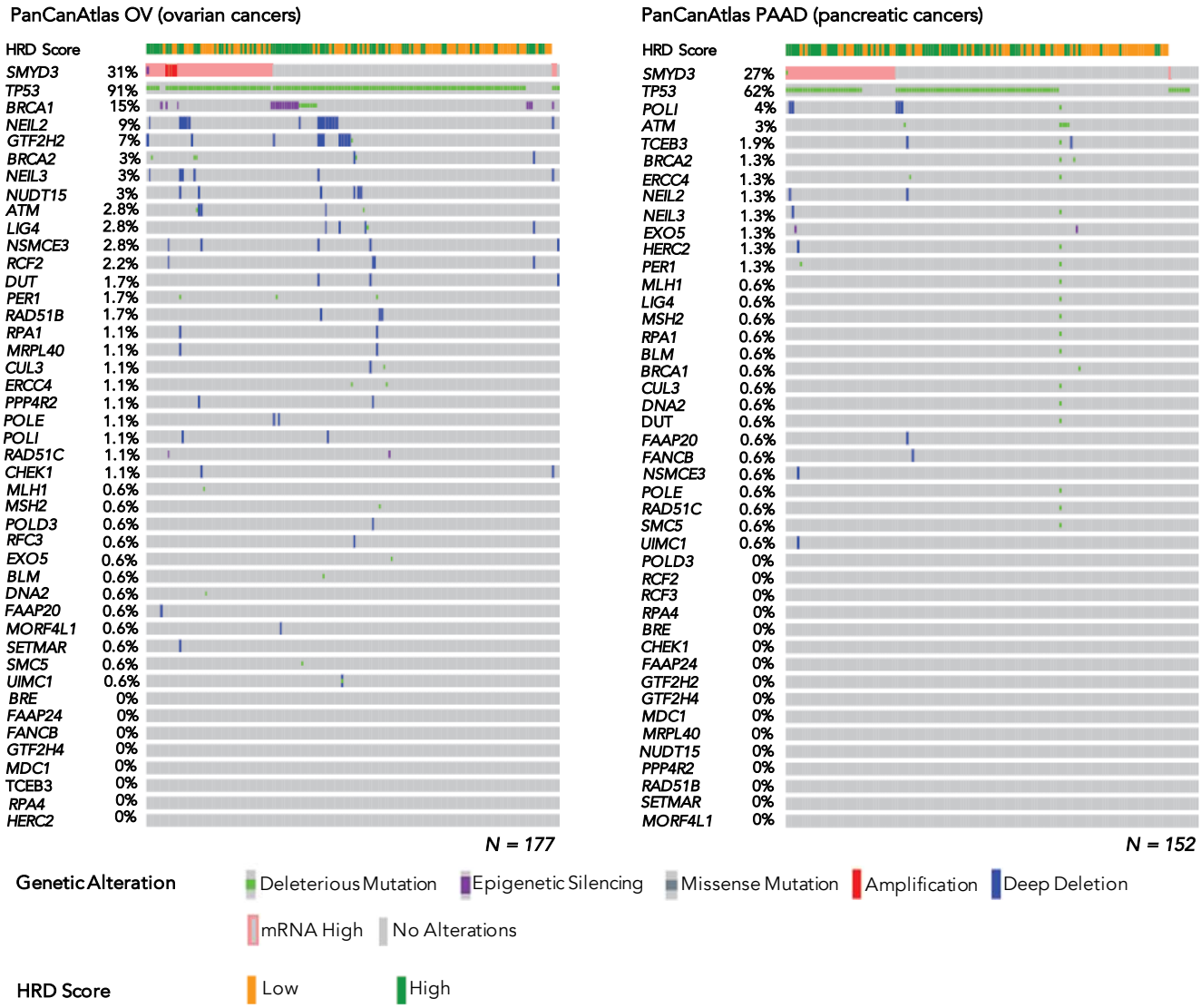

Figure S6. Oncoprint of *SMYD3* and HRD-associated genes in PanCanAtlas OV and PAAD tumors, (related to Figure 8).

Overall profiling of 177 OV and 152 PAAD tumors (columns) carrying alterations involving the *SMYD3* gene mRNA overexpression and deleterious mutations, deletions, and epigenetic silencing events for each HRD-associated gene (rows with gene names listed on the left). The association between tumors and the HRD score, [OV: low (≤ 44) and high (> 44); PAAD: low (≤17) and high (>17)], is represented as yellow and green bars, respectively. Grey boxes indicate the absence of alterations, and color/shape combinations corresponding to the various alteration types are indicated below the oncoprint. The frequency of each gene alteration in the oncoprint plot is indicated on the left.

	SMYD3 STATUS	IHC intensity	% positive cells	Localization
Proband (BC 39y)	p.Arg265His	3	95	cytoplasmic and nuclear
Father (BC 54y)	p.Arg265His	3	95	cytoplasmic
Paternal aunt (BC 43y)	p.Arg265His	3	95	cytoplasmic and nuclear
Paternal aunt (BC 50y)	Wild-type	3	70	cytoplasmic

Table S1: SMYD3 immunohistochemistry results in the analyzed BC family, (Related Figure 3).

	Gene 1	Gene 2	P-value	Q-value
BC	TP53	SMYD3	1.236261e-22	1.236261e-22
	BRCA1	SMYD3	3.264069e-09	6.215379e-09
	NEIL2	SMYD3	1.315987e-02	2.186762e-02
	HERC2	SMYD3	5.295595e-05	1.501736e-04
	ATM	SMYD3	1.214102e-03	2.226760e-03
	RAD51C	SMYD3	8.720251e-04	1.431774e-03
	BRCA2	SMYD3	5.848456e-04	1.016715e-03
COAD-READ	MLH1	SMYD3	2.5344277e-08	5.753839e-08
	ATM	SMYD3	1.019042e-04	1.101908e-04
	EXO5	SMYD3	3.064239e-09	7.806982e-09
	HERC2	SMYD3	2.499592e-06	3.315551e-04

Table S2: Results of mutual exclusivity analysis in PanCanAtlas BC and COAD-READ tumors, (Related Figure 8).

P-values and Q-values were obtained using the DISCOVER's mutual exclusivity test.

Transparent Methods

Clinical data

A high-risk, BRCA1/2 mutation-negative breast cancer (BC) family (Figure 3B) from the Italian Multicenter Study on Male BC (MBC) was selected for whole-exome sequencing (Rizzolo et al., 2019). The proband, a man affected by BC, was diagnosed at the age of 39 years with an estrogen/progesterone receptor-positive ductal carcinoma *in situ* and at the age of 48 years with an estrogen/progesterone receptor-positive invasive ductal carcinoma. His father was diagnosed with invasive BC at the age of 54 years; both paternal aunts were diagnosed with BC at 43 and 50 years, respectively.

Cell Lines

HEK-293, HCT116, MDA-MB-231, MDA-MB-468, MDA-MB-175, MDA-MB-415, MDA-MB-453, MDA-MB-436, MDA-MB-435, MDA-MB-361, HT29, MCF7, BT-474, BT-483, BT-20, DU4475, HCC1428, HCC1500, HCC1599, HCC38, HCC70, HCC202, HCC1954, HCC1143, HCC1187, HCC2218, HCC1806, HCC1419, HCC1937, HCC1569, DLD-1, LoVo, Caco2, OVCAR-3, A2780, SKOV-3, BxPC3, PK9, CAPAN-1, PANC-1, MIAPaCa-2, SW1990, SW480, T-47D, ZR-75-1, ZR-75-30, AU565, UACC-812, and SK-BR-3 cells lines were purchased from ATCC. CAL-85-1, CAL-148, CAL-51, CAL-120, EFM-19, EFM192A, Evsa-T, and HDQ-P1 cell lines were purchased from DSMZ. The U2OS cell line was kindly provided by Prof. Jeremy Stark. The SMYD3-KO MDA-MB-231 cell line was created using the CRISPR/Cas9 technology.
HEK-293, HCT116, MDA-MB-231, MDA-MB-468, HT29, MCF7, MDA-MB-231-SMYD3 KO, SW480, SW1990, OVCAR-3, SKOV-3, PANC-1, MIAPaCa-2, CAL-120, Evsa-T, SK-BR-3, HDQ-P1, and U2OS cells were cultured in DMEM high glucose (HG), without pyruvate (#11360-070, Gibco) with 10% FBS (#0270-106, Gibco) and 100 IU/ml penicillin-streptomycin (#15140-122, Gibco). HCC1428, MDA-MB-175, MDA-MB-415, MDA-MB-453, MDA-MB-436, MDA-MB-435, MDA-MB-361, UACC-812, CAL-85-1, CAL-148, CAL-51, BT-20, and BT-474 cells were maintained in the same conditions with 1% NEAA (#11140, Sigma Aldrich). LoVo cells were cultured in DMEM high glucose (HG) with 20% FBS and 100 IU/ml penicillin-streptomycin. Caco2 cells were maintained in the same conditions with 1% NEAA (#11140, Sigma Aldrich) and HEK-293 cells were supplemented with 1% pyruvate (#11360070, Gibco) and 1% NEAA (#11140, Sigma Aldrich). DLD-1, A2780, BxPC3, PK9, T-47D, ZR-75-1, ZR-75-30, EFM-19, EFM192A, HCC1428, HCC1500, HCC1599, HCC38, HCC70, HCC202, HCC1954, HCC1143, HCC1187, HCC2218, HCC1806, HCC1419, HCC1937, HCC1569, BT-483, AU565, DU4475, and CAPAN-1 cells were cultured in RPMI high glucose (HG), without pyruvate (#21875-034, Gibco) with 10% FBS (Gibco) and 100 IU/ml penicillin-streptomycin (Gibco). All cell lines were tested to be mycoplasma-free (#117048; Minerva Biolabs) at multiple times throughout the study. All cell culture was performed in a 37°C and 5% CO_2 incubator.

E. coli

Tuner™(DE3) Competent Cells (#70623) were obtained from Novagen and were grown in standard LB media. High-Efficiency DH5α Competent Cells (C2987H) obtained from New England Biolabs were used for all cloning experiments performed in this study. Cells were grown in standard LB media.

Chemicals

Neocarzinostatin (N9162), BCI-121 (SML1817), and Doxorubicin (D1515) were purchased from Sigma-Aldrich. KU60019 (S1570), and Olaparib (S1060) were purchased from SelleckChem. EPZ031686 (HY-19324) was purchased from MedChemExpress.
For each chemical, doses and treatment duration are indicated in the figure legends.

Peptides

Peptides were purchased from Proteogenix. Peptides were delivered in lyophilized form and obtained at a

purity of at least 95% with TFA removal and in the hydrochloride salt form. The peptides used in this work are listed below.
P1-tripeptide: NFF, P2-tripeptide: DFF, P3-tripeptide: LFF, P4-tripeptide: FFF, P5-tripeptide: QFF, P6-tripeptide: KFF, P7-tripeptide: NIF, P8-tripeptide: NYF, P9-tripeptide: NAF, P10-tripeptide: NDF, P11-tripeptide: NHF, P12-tripeptide: NNF, P13-tripeptide: NFI, P14-tripeptide: NFY, P15-tripeptide: NFA, P16-tripeptide: NFH, P17-tripeptide: NFW, P18-tripeptide: NFR, P19-tripeptide: NFK.

Plasmids

The plasmids described in the manuscript were generated with specific primers, as previously described (Nakatani Y et al., 2003**)**. Site-directed mutagenesis was performed using the Q5® Site-Directed Mutagenesis Kit (#E05545, New England Biolabs) according to the manufacturer's instructions.
The p3xFLAG-CMV14-SMYD3-WT construct was generated starting from the SMYD3 cDNA ORF Clone in Cloning Vector, Human (HG11217-M, Sino Biological), used as a template to amplify SMYD3. HindIII-SMYD3 FW *5′-CTAAAGCTTATGGAGCCGCTGAAG* and EcoRI-SMYD3 RV *5′-ATTACGAATTCTGGGATGCTCTGATGT* primers were used for the PCR. The SMYD3 fragment was cloned into the p3xFLAG-CMV14 EMPTY plasmid (E7908, Sigma) linearized with HindIII and EcoRI.
The pCMV14-SMYD3-WT-HAHA construct was generated starting from the pHAHA EMPTY (#12517, Addgene) plasmid, used as a template to amplify HAHA. KnpI-HA FW *5′-TGGTTGGTACCTGGATACGATGTTCCAGATTACGCT* and XbaI-stop-HA RV *5′-GGATCCTCTAGATGTATCTTATCATGTCTGGATCCGGC* primers were used for the PCR. The HAHA-stop codon fragment was cloned into the p3xFLAG-CMV14-SMYD3-WT plasmid linearized with KnpI and XbaI.
The pCMV14-SMYD3-R265H-FLAG construct was generated by site-directed mutagenesis, using SDM SMYD3 R265H FW *5′-P-GTGACTGTTTCCATTGCCAAACCCAGG* and SDM SMYD3 R265H RV *5′-P-ATTCAAAGCAGTACTGGTCCCTCAGC* primers.
The p3xFLAG-CMV14-SMYD3-WT-HAHA-SMYD3-R265H-FLAG construct was generated starting from p3xFLAG-CMV14-SMYD3-R265H, used as a template to amplify CMV14-SMYD3-R265H-FLAG. XhoI CMV FW *5′-AATCGCTCGAGTGATGCGGTTTTGGCAGTA* and XbaI-SMYD3 RV *5′-TACTCTAGAGGATGCTCTGATGTTGGC* primers were used for the PCR. The CMV14-SMYD3-R265H-FLAG fragment was cloned into the pCMV14-SMYD3-WT-HAHA plasmid linearized with XhoI and XbaI.
pCS2-MYC-SMYD3-WT was generated as previously described in Proserpio et al., 2013.
pCDNA-FLAG-CHK2 was generated as previously described in Zannini et al., 2003.
GST-BRCA2 fragments (B2-1 to B2-9) cloned into the pGEX-4T3-GST vector were kindly provided by Professor Ashok Venkitaraman (MRC Cancer Unit, Cambridge, UK). GST-ATM fragments (A1 to A8) cloned into the pGEX-4T2-GST vector were kindly provided by Professor Titia de Lange (The Rockefeller University, New York, USA). GST-HSP90 C (616-736) (#22483), pCDNA3.1(+)-HIS-FLAG-ATM (#31985) and pET28-MHL-SMYD3-WT (#32048) were purchased from Addgene**.**

Cell transfection and RNA interference

U2OS cells were co-transfected with pCBASceI (#26477, Addgene) and p3xFLAG-CMV14-SMYD3-WT or p3xFLAG-CMV14-SMYD3-R265H using Lipofectamine 3000 (#L3000015, Thermo Fisher Scientific) according to the manufacturer's instructions.
MDA-MB-231 cells were transiently transfected with mammalian expression plasmids using fectamine 3000 (L3000015, Thermo Fisher Scientific) according to the manufacturer's instruction. For RNA interference, MDA-MB-231 cells were transfected with 50 nM validated siRNAs (Eurofins) directed against SMYD3 by using the HiPerfect reagent (#301704, QIAGEN) according to the manufacturer's instructions. siCTRL (Eurofins) was used as a non-silencing control. siRNA sequences used in this study:
siSMYD3: 5'-GAU UGA AGA UUU GAU UCU A
siCTRL: 5'-GCG UUG CUC GGA UCA GAA A

CRISPR/Cas9 system

The CRISPR/Cas9 reporter vector, GeneArt CRISPR Nuclease Vector Kit (#A21175, Invitrogen), was used according to the manufacturer's instructions. The *SMYD3* gene was analyzed with the CRISPR Search and

Design Tool (Thermo Fisher Scientific), which identified three different gRNA: gRNA1 top strand *5′-TTGCACACCGTGTACGCCAgtttt*, gRNA1 bottom strand *5′-TGGCGTACACGGTGTGCAAGcggtg,* gRNA2 top strand *5′-TTGGCGTACACGGTGTGCAgtttt,* gRNA2 bottom strand *5′-GCACACCGTGTACGCCAAGcggtg,* gRNA3 top strand *5′-AGTTCGCAACCGCCAAGAGgtttt,* gRNA3 bottom strand *5′-CTCTTGGCGGTTGCGAACTTcggtg.*
MDA-MB-231 cells were transfected with all-in-one expression vector Cas9-CD4^{+}-SMYD3 gRNA using Lipofectamine 3000 (L3000015, Thermo Fisher Scientific) according to the manufacturer's instruction. After 48 h MDA-MB-231 CD4^{+} cells were enriched using the Dynabeads CD4 Positive Isolation Kit (11331D, Thermo Fisher) according to the manufacturer's instructions. Isolation of clonal populations was performed with agarose-based cloning rings (#C1059, Sigma). Cell clones were tested for site-specific loss of function alterations by PCR, using SMYD3 gRNA sequencing FW *5′-AGCCCGTGAGACGCCCGCTGCTGG* and SMYD3 gRNA sequencing RV *5′-GAAAAGTTCGCAACCGCCAA*. Sequencing products were purified using the Dye Ex 2.0 Spin Kit (#63204, QIAGEN) and sequenced on an ABI PRISM 310 Genetic Analyzer (Applied Biosystems).

Recombinant protein expression/purification

Tuner™(DE3) Competent Cells, transformed with different constructs, were grown in Luria Broth medium with Ampicillin (A9518, Sigma), Chloramphenicol (C0378, Sigma), and 0,5 mg/ml L-(+)-Arabinose (A3256, Sigma) and induced with 1 mM IPTG when they reached the optical density of 0.6 (A600) at 37°C, for 3 h. Cells were then collected by centrifugation, and pellets were lysed with B-PER lysis buffer (#78248, Thermo Fisher Scientific). The lysate was centrifuged at 20,000 × *g* for 20 min at 4°C. Recombinant protein expression was confirmed by SDS-PAGE. GST-Fusion proteins were purified by Pierce Glutathione Magnetic Agarose Beads (78601, Thermo Fisher Scientific) according to the manufacturer's instructions. GST-fused proteins were evaluated and quantified by SDS-PAGE. HIS-Fusion proteins were purified by Dynabeads HIS-Tag Isolation and Pulldown (10104D, Thermo Fisher Scientific) according to the manufacturer's instructions. HIS-fused proteins were evaluated and quantified by SDS-PAGE.

Immunoblotting

Whole-cell extracts were obtained from cells collected and homogenized in lysis buffer (50 mM Tris-HCl pH 7.4, 5 mM EDTA, 250 mM NaCl, and 1% Triton X-100) supplemented with protease and phosphatase inhibitors (Roche). Nuclear fractions were obtained by using the Nuclear Extraction Kit (#ab113474, Abcam) according to the manufacturer's instructions. 20 µg of protein extracts from each sample were denatured in Laemmli sample buffer and loaded into an SDS-poly-acrylamide gel for immunoblot analysis. Primary antibodies used: 53BP1 (#4937, Cell Signaling), ATM (#2873, Cell Signaling), ACTIN (#3700, Cell Signaling), BRCA2 (OP95, Merck), CHK2 (#6334, Cell Signaling), FLAG M2 (F1804, SIGMA), GAPDH (#2118, Cell Signaling), GST (#2625, Cell Signaling), HA-tag (H3663, SIGMA), MYC-tag (#2278, Cell Signaling), p-Ser/Thr ATM/ATR (#2851), PARP p85 Fragment (G7341, Promega), pATM (Ser1891) (#5883 Cell Signaling), polyHistidine (H1029, Sigma), RAD51 (#8875, Cell Signaling), SMYD3 (D2Q4V) (#12859, Cell Signaling), yH2AX (#9718, Cell Signaling) and LAMIN B1 (#12586S, Cell Signaling). Rabbit IgG HRP and Mouse IgG HRP (#NA934V, #NA931V, GE Healthcare) were used as secondary antibodies and revealed using the ECL-plus chemiluminescence reagent (GE Healthcare). Densitometric evaluation was performed by ImageJ software (Schneider et al., 2012).

Co-immunoprecipitation (Co-IP)

Cells were lysed with the Nuclear Extraction Kit (ab13474, Abcam), according to the manufacturer's instructions. 10% of the nuclear fractions was used as input. 1 µg of each antibody was coupled to Dynabeads Protein A (10002D, Thermo Fisher Scientific) or G (10004D, Thermo Fisher Scientific) in 100 µl of 0.01% Tween20-1X PBS for 45 min at room temperature on a rocking platform. Nuclear fractions were incubated with antibody-Dynabeads Protein A or G complexes for 1 h at room temperature on a rocking platform. Immunocomplexes were washed extensively, boiled in Laemmli sample buffer, and subjected to SDS-PAGE and immunoblot analysis. Primary antibodies used: MYC-tag (#2278, Cell Signaling), BRCA2 (OP95, Merk Millipore), FLAG (F1804, Sigma) and ATM (#2873, Cell Signaling). IgG was used as a negative control.

For endogenous co-immunoprecipitation, cells were lysed with the Nuclear Extraction Kit (ab13474, Abcam), nuclear fractions were digested or not in 1x Micrococcal Nuclease Reaction buffer with 0,1 U/µL of MNase (M0247S, New England Biolabs) for 5 min at 37°C. 1 µg of SMYD3 antibody (#12859, Cell Signaling Technologies) was coupled to Dynabeads Protein A (10002D, Thermo Fisher Scientific) and co-immunoprecipitation was carried on as described above.

DR-GFP reporter assay

U2OS-DR-GFP cells were seeded in 6 cm cell culture plates ($1x10^6$ cells/plate) and after 24h they were transfected with SceI-BFP, SceI-BFP+SMYD3_WT and SceI-BFP+SMYD3_R265H expressing vectors, using Lipofectamine 3000 transfection reagent (L3000015, Thermo Scientific, USA) according to manufacturer's instructions. After 24 h, cells were detached from plates by using 0.25% Tyripsin-EDTA (TD-4049-100, Sigma,USA), centrifuged at 1000 rpm x 10 min and suspended in an appropriate volume of cold flow cytometry buffer (phosphate buffer saline supplemented with 1% BSA). Cells were analyzed by using FACS Aria II fluorescence activated cell sorter (Beckton Dickinson, USA).

Annexin V staining

Briefly, 1×10^6 cells were cultured in 6-well plates (Corning Costar, Corning) for 72 h at 37°C, 5% CO2, with complete medium. After 24 h, cells were pre-treated or not for 48 h with BCI-121 or EPZ031686 and then treated or not with olaparib and/or with BCI-121 or EPZ031686 for another 24 h. 2×10^4 cells/plate were collected and resuspended in 1X PBS-1% FBS, then the Muse Annexin V and Dead Cell reagent was added to each tube (MCH100105, Luminex). Cells were incubated at room temperature for 20 min in the dark. Flow cytometry was performed using the Guava Muse Cell Analyzer. Cells were considered apoptotic if they were Annexin V+/PI- (early apoptotic) and Annexin V+/PI+ (late apoptotic). Each analysis was performed evaluating at least 2000 events using the assay-specific software module included in the Guava Muse Cell Analyzer instrument.

Colony formation assay

Colony formation assays were performed as previously described (Germani et al., 2014). Briefly, cells were cultured in 24-wells in the presence or absence of the indicated drugs. After 72 h, media were discarded and cells were washed twice with 1X PBS. An aliquot of 2 ml of Coomassie brilliant blue (#161-0400, BIORAD) was added into each dish for 5 min and then cells were washed with 1X PBS to remove excess Coomassie. Plates were dried at room temperature. Percent cell growth inhibition at each concentration was quantified by densitometric evaluation using ImageJ software (Schneider et al., 2012).

Immunofluorescence and foci counting

53BP1 (NB100-304, Novus Biologicals), γH2AX (05-636 Merck Millipore), FLAG (F1804, Sigma Aldrich), and RAD51 (#8875, Cell Signaling) foci were stained by immunofluorescence. Cells were grown on glass coverslips, treated as indicated for each experiment, and then fixed with 3% paraformaldehyde and 2% sucrose in 1X PBS for 10 min and permeabilized with 20 mM HEPES pH 7.6, 50 mM NaCl, 3 mM MgCl2, 300 mM sucrose, 0.2% Triton-X-100 for 5 min at room temperature. Glass coverslips were then blocked in 1X PBS, 3% BSA for 30 min, stained with primary antibody for 2 h at room temperature, then with Alexa Fluor secondary antibodies for 1 h at room temperature. Coverslips were mounted with medium anti-fading-containing DAPI to stain nuclei. Foci were scored by fluorescence microscopy using a 100X magnification objective and digital image acquisition on a Nikon Eclipse E1000 equipped with a DS-U3 CCD camera. The percentage of 53BP1 foci was calculated as follows: % residual damage = [(foci t_{24h}-foci t_0)/ (foci $t_{1.75h}$-foci t_0)] x 100.

Cell viability and cell death

Cell viability and cell death were assessed by counting. Briefly, supernatants (containing dead/floating cells) were collected. Cell pellets were resuspended in 1X PBS and 10 µl were mixed with an equal volume of 0.01% Trypan blue solution (T8154, Sigma-Aldrich). Viable cells (unstained, trypan blue-negative cells) and

dead cells (stained, trypan blue-positive cells) were counted with a phase-contrast microscope, and the percentages of viable and dead cells were calculated.

DNA/RNA extraction, sequencing, and analysis

DNA was extracted from both whole blood samples and microdissected FFPE sections of breast cancer tissue with commercial kits as previously reported (Silvestri et al., 2017).
Whole-exome sequencing of germline DNA samples from breast cancer tissue and subsequent data analysis were performed as previously described (Silvestri et al., 2017). Candidate variants were validated in germline and tumor DNA samples by double-stranded Sanger sequencing.
RNA was extracted from microdissected FFPE tumor sections using the MiReasy FFPE kit (217504, Qiagen) according to the manufacturer's instructions. RNA quality and quantity were assessed on a 2100 Bioanalyzer instrument (Agilent) (Wang et al., 2012). Libraries were prepared using the TruSeq RNA Access Library Prep kit (RS-301-2001, Illumina) according to the manufacturer's instructions. RNA-sequencing (75x2 bp) was performed on an Illumina NextSeq platform. A tailored bioinformatic pipeline including tools such as FastQC for quality control, STAR (version 2.5.1a) for alignment, and RSeQC-FPKM for counting reads was applied. Absolute quantification of transcripts (genes with all isoforms) was expressed in Fragments Per Kilobase of transcript per Million mapped reads (FPKM). The GATK Best Practices workflow for SNP and indel calling on RNA-seq data was used to evaluate the expression of variant alleles (Tian et al., 2016).

Immunohistochemistry

Tissue specimens were formalin-fixed in 4% buffered formalin and paraffin-embedded. Sequential sections (3 μm) were cut and used for morphological studies [stained with hematoxylin and eosin (HE)] and immunohistochemical analysis.
Sections were dewaxed and rehydrated in dH_2O. Endogenous peroxidase activity was blocked by incubation in 3% hydrogen peroxide for 10 min. Antigen retrieval was conducted in 10 mM sodium citrate buffer (pH 6.0) for 15 min. Sections were incubated overnight with the primary antibody, anti-SMYD3 (ab183498, Abcam, 1:200 dilution). Then, they were incubated with secondary biotinylated antibody and subsequently with streptavidin-biotin-peroxidase (UltraTek HRP Anti-Rabbit, Scy Tek). Samples were developed with DAB (ACH500, Scy Tek), counterstained with hematoxylin, and mounted with permanent mounting media. Negative controls were used in each experiment. SMYD3 immunoreactivity was evaluated by a semiquantitative approach by two independent pathologists, in a blinded manner, who scored the percentage of SMYD3-stained cells and the intensity of the staining (0: absent, 1: mild and focal, 2: moderate, 3: intense and diffuse).

Chromatin immunoprecipitation (ChIP)

Chromatin isolated from U2OS cells co-transfected with pCBASceI and p3xFLAG-CMV14-SMYD3-WT or p3xFLAG-CMV14-SMYD3-R265H was subjected to ChIP. Briefly, cells were cross-linked in 1% formaldehyde (F8775, Sigma Aldrich) for 10 min. After blocking cross-links with 0.125 M glycine for 5 min and washing with PBS, the pellet was resuspended in Farnham buffer (5 mM PIPES pH 8.0; 85 mM KCl; 0.5% NP-40). Cells were lysed in RIPA buffer (1× PBS; 1% NP-40; 0.5% sodium deoxycholate; 0.1% SDS). Chromatin was sonicated to a fragment length of about 1 kb and immunoprecipitated with 5 μg of rabbit IgG, anti-SMYD3 (NBP1-79393, NovusBio) or anti-RAD51 (14B4, cat. NB100-148, NovusBio) antibodies.
ChIP primers used:
DR-GFP+1300 FW: 5'- CCCCCGTAGCTCCAATCCTT
DR-GFP+1300 RV: 5'-CCAGGAGCGGATCGAAATTG
hChIP UbiquitB FW: 5'-GAAGGAAGAGAAGCGCATAGAGGAGAA
hChIP UbiquitB RV: 5'-CTCATAGCCGTAAGAAAGGCTCCTAAA
Quantitative real-time PCR was performed using SYBR green IQ reagent (Bio-Rad Laboratories) with the CFX Connect detection system (Bio-Rad Laboratories).

Surface plasmon resonance (SPR)

Direct binding assays were conducted employing flow-based SPR biosensor X100, (BIAcore, GE Healthcare) and data analysis was performed employing Scrubber or BIAevaluation software version 4.1. Recombinant human full-length SMYD3 was produced and purified in-house following a previously developed protocol (Peserico et al., 2015). Immobilization of SMYD3 on CM5 sensor chips was performed following a previously described amine-coupling procedure (Fabini et al., 2019). Briefly, using Hepes buffer saline (HBS) as running buffer, a 1:1 mixture of 0.4 M N-(3-Dimethylaminopropyl)-N'-ethylcarbodiimide (EDC) and 0.1 M N-hydroxy succinimide (NHS) was injected for 7 min over the sensor surface followed by 10 min injection of the recombinant human full-length SMYD3 diluted to 100 µg/ml. Remaining active esters were quenched by switching the running buffer to tris buffer saline containing 0.05% Tween-20 (TBS-T) supplemented with 2 mM dithiothreitol (DTT) and 2% DMSO. During the immobilization procedure, the flow rate was set at 10 µl/min. After the immobilization process, the surface was left to stabilize overnight to remove all tightly bound S-adenosyl methionine (SAM) which co-purifies with the protein. The whole process resulted in c.a. 8000 RU (Response Units) of SMYD3 covalently attached to the surface. For all performed experiments, the analysis temperature was set to 15°C. Interaction of tripeptides with immobilized SMYD3 was investigated using a 90 µl/min flow rate. Association was monitored for 30s and dissociation for 120s. All responses returned to baseline quickly after injection stopped, thus no regeneration procedure was necessary. A double-reference approach was used as negative control: the SPR signal was recorded upon injection of each tripeptide over the sensing surface bearing the immobilized SMYD3 and was corrected by the signal recorded in the reference cell and that of a blank solution. Reference cell allows accounting for non-specific interactions while signals recorded upon injections in both cells of a blank solution accounted for optical interference. RU values measured at the end of the injection phase were normalized for the molecular weight (MW) of each tripeptide to achieve MW-adjusted RUs. Interactions of tripeptides with immobilized SMYD3 were monitored both in SAM-free and SAM-supplemented buffer. SAH (S-adenosyl-homocysteine) was used as a positive control compound in the first instance while a 26-amino acid peptide, based on MAP3K2 sequence 249-274, was used in the latter. The total number of replicates was 2.

***In vitro* pull-down assay**

HIS-SMYD3-WT recombinant human protein was incubated with nine GST fusion proteins, designated B2-1 to B2-9, that span the entire coding region of BRCA2, or with eight GST fusion proteins, designated A-1 to A-8, that span the entire coding region of ATM, or with recombinant human CHK2 protein (ab42604, Abcam). HSP90 C (616-736) GST fusion protein was used as a positive control. HIS-SMYD3-WT recombinant protein (500 ng) and GST fusion proteins (200 ng) were incubated for 1 h at 4°C on a rocking platform for *in vitro* binding. These fusion proteins were precipitated by Dynabeads HIS-Tag Isolation and Pulldown (Thermo Fisher Scientific) according to the manufacturer's instructions, then washed extensively in buffer A (20 mM Tris-HCl pH 8, 150 mM KCl, 5 mM MgCl2, 0.2 mM EDTA, 10% glycerol, 0.1% NP-40) containing fresh inhibitors and 1 mM DTT. Afterward, the precipitates were resolved on 10% SDS-PAGE and subjected to immunoblot analysis. Primary antibodies used: polyHistidine (H1029, Sigma) and GST (#2625, Cell Signaling). Rabbit IgG HRP and Mouse IgG HRP (#NA934V, #NA931V, GE Healthcare) were used as secondary antibodies and revealed using the ECL-plus chemiluminescence reagent (GE Healthcare).
For the competition assay, 500 ng of HIS-SMYD3-WT recombinant protein and 200 ng of GST-BRCA2 B2-4 or GST-ATM A-8 fusion proteins were incubated for 1 h at 4°C on a rocking platform in the presence of escalating doses (0, 1, 5, 25, 125, 625 mM) of the purified P1 and P10 tripeptides, respectively. Bound proteins were precipitated and resolved as described above.

ADP luminescent assay

Analysis of ATM kinase activity was performed using a luminometric kinase assay by varying the concentration of ATP using the ADP-Glo reagents (#V6930, Promega). This luminescent ADP detection assay measures kinase activity by quantifying the amount of ADP produced during a kinase reaction. Briefly, ATM active protein (100 ng, #14-933 Millipore) was assayed in a kinase reaction buffer containing 40 mM Tris (pH 7.5), 20 mM MgCl2, 0.1 mg/ml BSA, varying concentrations of ATP, and 500 ng of human recombinant SMYD3-WT or SMYD3-R265H. After 30 min of incubation, an equal volume of ADP-Glo reagent was added to stop the kinase reaction and deplete the remaining ATP. Then, kinase detection reagent was added to convert ADP to ATP, which was determined by a luciferase/luciferin reaction. The generated

luminescence was measured using a luminometer. Each data point was collected in triplicate and the result is shown as fold change on active-ATM only.

Prediction analysis

P-tripeptide screening was performed *in silico* using the Uniprot Peptide search tool (https://www.uniprot.org/peptidesearch/) to identify potential candidates as new SMYD3 interactors. Each P-tripeptide was searched in all human proteins annotated in the Uniprot database (analysis performed in December 2018) and 8,650 proteins showed at least one identified tripeptide. Then, we analyzed the subset of all human proteins showing ≥ 4 P-tripeptide occurrences (214 proteins) for their biological function based on the functional annotation reported in the related Uniprot entry and in the Reactome database (i.e. HR pathway, Reactome id: R-HSA-5685942; https://reactome.org/; Fabregat et al., 2018; Jassal et al., 2020). Of note, we found that 24 proteins showing ≥4 P-tripeptide occurrences are involved in DNA repair and S-phase checkpoint pathways.

In silico prediction of SMYD3 phosphorylated sites was performed using three different tools: PhosphoELM (http://phospho.elm.eu.org/, Dinkel et al., 2011), DISPHOS (http://www.dabi.temple.edu/disphos/, Iakoucheva et al., 2004) and NetPhos (http://www.cbs.dtu.dk/services/NetPhos/, Bloom, et al., 2004). This analysis identified T268 as the best target site for phosphorylation by ATM.

TCGA PanCanAtlas data source/meta-analysis

The analysis of genomic alterations of PanCanAtlas breast invasive carcinoma (BC), colon and rectum adenocarcinoma (COAD, READ), pancreatic adenocarcinoma (PAAD) and ovarian serous cystadenocarcinoma(OV) tumors was performed using a published study carried out by integrating data on somatic truncating and missense mutations, copy number deletions defined by GISTIC, and epigenetic silencing events by The Cancer Genome Atlas (TCGA) DNA Damage Repair Analysis Working Group (Knijnenburg et al., 2018). The available binary calls for each event class for a curated list of 276 genes encompassing all major DNA repair pathways were used to assess the prevalence of 43 DNA damage repair (DDR) gene alterations (*LIG4*, *MLH1*, *MSH2*, *POLD3, RFC2*, *RFC3*, *RPA1*, *RPA4*, *ATM*, *BLM*, *BRCA1*, *BRCA2*, *BRE*, *CHEK1*, *CUL3*, *DNA2*, *DUT*, *ERCC4*, *FAAP24*, *FAAP20*, *FANCB*, *GTF2H2*, *GTF2H4*, *MDC1*, *MRPL40*, *NEIL2*, *NEIL3*, *NSMCE3*, *NUDT15*, *PER1*, *POLE*, *POLI*, *PPP4R2*, *RAD51B*, *RAD51C*, *SETMAR*, *SMC5*, *TCEB3*, *TP53*, *UIMC1*, *EXO5*, *MORF4L1*, and *HERC2*) with a significant positive homologous recombination deficiency (HRD) determined using Bayesian ridge regression to model HRD scoring as a function of DDR gene alterations. We retrieved from the same published article the HRD score, a measure obtained by combining three separate metrics of genomic scarring (HRD loss of heterozygosity, large scale transition, and the number of telomeric imbalances). We defined BC, COAD-READ, PAAD, and OV as low HRD scoring if the HRD score was below or equal the median within the relevant cancer type. The website cBioPortal (https://www.cbioportal.org; Gao et al., 2013; Cerami et al.,2012) was used for the meta-analysis. Somatic mutations, copy number alterations, and RSEM processed and Z-score RNA-Seq v2 gene expression data from PanCanAtlas BC (N=981), COAD-READ (N=459), PAAD (N=152), and OV (N=177) tumors that were comprehensively and systematically analyzed for 276 DDR genes were downloaded from cBioPortal (http://www.cbioportal.org) to characterize *SMYD3* somatic alterations. Patients were stratified based on *SMYD3* Z-score and the third quartiles were identified as high SMYD3 (BC, q3 SMYD3 Z-score ≥ 1.06, N=245), (COAD-READ, q3 SMYD3 Z-score ≥ 0.41, N=126), (PAAD, q3 SMYD3 Z-score ≥ 0.41, N=41), (OV, q3 SMYD3 Z-score ≥ 0.65, N=52).

Mutual exclusion analysis

Mutual exclusivity between *SMYD3* and HRD-associated genes was evaluated using the DISCOVER analysis tool (Sander et al., 2016). Overexpression of *SMYD3* mRNA and deleterious alterations of 43 HRD-associated genes from 981 BC, 459 COAD-READ, 152 PAAD, and 177 OV tumors were combined into a single *NxM* binary data matrix for each cancer type, where each cell value $V_{i,j}$ ($i = 1 \ldots N$ *[Number of genes]*, $j = 1 \ldots M$ *[Number of tumors]*) indicated the status of gene i in tumor j. $V_{i,j} = 1$ if gene i is mutated in tumor j and 0 otherwise. The alteration status of all genes across all tumors for each cancer type was used to generate a null distribution for background alternation rate estimation. Finally, we computed pairwise mutual

exclusivity between any two genes mutated in more than two tumors, taking the null distribution into account.

Cell line mutational analysis

Somatic mutations and copy number alteration data of key HR-related genes (BRCA1, BRCA2, CHEK2, ATM, RAD51B, RAD51C, and RAD51D) were retrieved from the Cancer Cell Line Encyclopedia (CCLE, https://portals.broadinstitute.org/ccle; Ghandi et al., 2019) and the Catalogue of Somatic Mutation in Cancer (COSMIC, https://cancer.sanger.ac.uk/cosmic; Tate et al., 2019) databases to assess the mutational status of BC cell lines (CCLE: HCC70_BREAST, MCF7_BREAST, BT474_BREAST, HCC1428_BREAST, MDAMB231_BREAST, MDAMB468_BREAST), colon cancer cell lines (CCLE: LOVO_LARGE_INTESTINE, HT29_LARGE_INTESTINE, HCT116_LARGE_INTESTINE, SW480_LARGE_INTESTINE, CaCo2_LARGE_INTESTINE, DLD1_LARGE_INTESTINE), ovarian cancer cell lines (CCLE: NIHOVCAR3_OVARY, A2780_OVARY, SKOV3_OVARY,), and pancreatic cancer cell lines (CCLE: CAPAN1_PANCREAS, MIAPACA2_PANCREAS, PANC1_PANCREAS, BXPC3_PANCREAS; COSMIC: PK-9).

QUANTIFICATION AND STATISTICAL ANALYSIS

Data were analyzed and plotted using Microsoft Excel and GraphPad Prism softwares. Statistical analysis was performed using Student's t-test or one-way ANOVA followed by a Dunnett test. Differences were considered significant when $p \leq 0.05$. At least three independent experiments were performed for all of the assays.

Supplemental References

Blom, N., Sicheritz-Pontén, T., Gupta, R., Gammeltoft, S., and Brunak, S. (2004). Prediction of post-translational glycosylation and phosphorylation of proteins from the amino acid sequence. Proteomics 4, 1633–1649.

Cerami E., Gao, J., Dogrusoz, U., Gross, B.E., Sumer, S.O., Aksoy, B.A, Jacobsen, A., Byrne, C.J., Heuer, M.L., Larsson, E., et al. (2012). The cBio cancer genomics portal: an open platform for exploring multidimensional cancer genomics data. Cancer Discov. 2, 401–404.

Dinkel, H., Chica, C., Via, A., Gould, C.M., Jensen, L.J., Gibson, T.J., and Diella, F. (2011). Phospho.ELM: a database of phosphorylation sites-update 2011. Nucleic Acids Research. 39, D261–D267.

Fabini E., Manoni E., Ferroni C., Del Rio, A., and Bartolini M. (2019). Small-molecule inhibitors of lysine methyltransferases SMYD2 and SMYD3: current trends. Future Med. Chem. 11, 901–921.

Fabregat A., Jupe S., Matthews L., Sidiropoulos K., Gillespie M., Garapati P., Haw, R., Jassal B., Korninger F., May B., Milacic, M., et al.(2018). The Reactome Pathway Knowledgebase. Nucleic Acids Res. 46, D649–D655.

Germani, A., Matrone, A., Grossi, V., Peserico, A., Sanese P., Liuzzi M., Palermo R., Murzilli S., Campese A.F., and Ingravallo G., et al. (2014). Targeted therapy against chemoresistant colorectal cancers: Inhibition of p38α modulates the effect of cisplatin in vitro and in vivo through the tumor suppressor FoxO3A. Cancer Lett. 344, 110–118.

Ghandi, M., Huang, F.W., Jané-Valbuena, J., Kryukov, G.V., Lo, C.C., McDonald III, E.R., Barretina, J., Gelfand, E.T., Bielski, C.M., Li, H., et al. (2019). Next-generation characterization of the Cancer Cell Line Encyclopedia. Nature 569, 503–508.

Iakoucheva, L.M., Radivojac, P., Brown, C.J., O'Connor,T.R., Sikes, J.G., Obradovic, Z., and Dunker, A.K. (2004). Intrinsic disorder and protein phosphorylation. Nucleic Acids Res. 32, 1037–1049.

Jassal, B., Matthews, L., Viteri, G., Gong, C., Lorente, P., Fabregat, A., Sidiropoulos, K., Cook, J., Gillespie, M., Haw, R., et al. (2020). The reactome pathway knowledgebase. Nucleic Acids Res. 48, D498–D503.

Knijnenburg, T.A., Wang, L., Zimmermann, M.T., Chambwe, N., Gao, G.F., Cherniack, A.D., Fan, H., Shen, H., Way, G.P., Greene CS, et al. (2018). Genomic and Molecular Landscape of DNA Damage Repair Deficiency across The Cancer Genome Atlas. Cell Rep. 23, 239–254.e6.

Nakatani Y., and Ogryzko, V. (2003). Immunoaffinity purification of mammalian protein complexes. Methods Enzymol. 370, 430–444.

Peserico, A., Germani, A., Sanese P., Barbosa, A.J., Di Virgilio V., Fittipaldi R., Fabini E., Bertucci C., Varchi G., Pat Moyer M., et al. (2015). A SMYD3 Small-Molecule Inhibitor Impairing Cancer Cell Growth. J. Cell. Physiol. 230, 2447–2460.

Proserpio, V., Fittipaldi, R, Ryall, J.G., Sartorelli, V., and Caretti, G. (2013). The methyltransferase SMYD3 mediates the recruitment of transcriptional cofactors at the myostatin and c-Met genes and regulates skeletal muscle atrophy. Genes Dev. 27, 1299–1312.

Rizzolo, P., Zelli, V., Valentina Silvestri, V., Virginia Valentini, V., Zanna, I., Bianchi, S., Masala, G., Spinelli, A.M., Tibiletti, M.G., Russo, A., et al. (2019). Insight into genetic susceptibility to male breast cancer by multigene panel testing: Results from a multicenter study in Italy. Int. J. Cancer. 145, 390–400.

Sander, C., Martens, J.W.M., and Lodewyk F. A. (2016). Wessels A novel independence test for somatic alterations in cancer shows that biology drives mutual exclusivity but chance explains most co-occurrence. Genome Biol. 17, 261.

Schneider, C.A., Rasband, W.S., and Eliceiri, K.W. NIH Image to ImageJ: 25 years of image analysis. (2012). Nat. Methods. 9, 671–675.

Silvestri, V., Zelli, V., Valentini, V. Rizzolo, P., Navazio, A.S., Coppa, A., Agata, S., Oliani, C., Barana, D., Castrignanò, T., et al. (2017). Whole-exome sequencing and targeted gene sequencing provide insights into the role of PALB2 as a male breast cancer susceptibility gene. Cancer 123, 210–218.

Tate, J.G., Bamford, S., Jubb, H.C., Sondka, Z., Beare D.M., Bindal, N., Boutselakis, H., Cole, C.G., Creatore, C., Dawson, E., et al. (2019). COSMIC: the Catalogue Of Somatic Mutations In Cancer. Nucleic Acids Res. 47, D941–D947.

Tian, S., Yan, H., Kalmbach, M., and Slager, S.L. (2016). Impact of post-alignment processing in variant discovery from whole exome data. BMC Bioinformatics. 17, 403.

Wang, L., Wang, S., and Li, W. (2012). RSeQC: quality control of RNA-seq experiments. Bioinformatics (Oxford, England). 28, 2184–2185.

Zannini, L., Lecis, D., Lisanti, S., Benetti, R., Buscemi, G., Schneider, C., and Delia D. (2003). Karyopherin-alpha2 protein interacts with Chk2 and contributes to its nuclear import. J. Biol. Chem. 278, 42346–42351.